Intrinsic excitability mechanisms of neuronal ensemble formation

Tzitzitlini Alejandre-García, Samuel Kim, Jesús Pérez-Ortega and Rafael Yuste

Neurotechnology Center, Dept. Biological Sciences, Columbia University, New York, NY 10027, USA

Running Head: Mechanisms of neuronal ensembles

Correspondence to:
Rafael Yuste
902 NWC Building 550 West 120 Street, Box 4822, New York, NY, 10027.
Email: rmy5@columbia.edu

Number of pages (Title page, Abstract, Introduction, Methods, Results, Discussion): 30

Number of figures: 9

Number of words: Abstract (), Introduction (), Discussion ()

Conflict of Interest: The authors declare no competing financial interests

Acknowledgments: We thank James Holland, for his assistance and members of the Yuste Lab for useful comments. Supported by R01EY011787 and R01MH115900. T.A and J.P. have postdoctoral fellowships from the National Council of Science and Technology from Mexico (CONACYT). The authors have no competing financial interests to declare. S.K. and R.Y. conceived the project. S.K. and T.A. performed experiments and T.A. and R.Y. wrote the paper. T.A., S.K. and J.P. analyzed the data. All authors planned experiments, discussed results and edited the paper. R.Y. assembled and directed the team and secured funding and resources.

Significance Statement:

We investigated the synaptic and cellular mechanisms underlying the formation of neuronal ensembles, i.e., spontaneously coactive groups of neurons. Using *in vitro* electrophysiology and optogenetic in slices of mouse neocortex we replicated a protocol that generates ensembles *in vivo*. After optogenetic and electrical stimulation, we observed biphasic synaptic plasticity and, unexpectedly, major increases in excitability, input resistance, and reductions in firing threshold. The increased excitability can explain the observed synaptic plasticity. Our results reveal a major role for intrinsic excitability in the establishment of neuronal ensembles.

Abstract

Neuronal ensembles are coactive groups of cortical neurons, found in spontaneous and evoked activity, that can mediate perception and behavior. To understand the mechanisms that lead to the formation of ensembles, we co-activated optogenetically and electrically layer 2/3 pyramidal neurons in brain slices from mouse visual cortex, in animals from both sexes, replicating *in vitro* an optogenetic protocol to generate ensembles *in vivo*. Using whole-cell and perforated patch-clamp pair recordings we find that, after optogenetic or electrical stimulation, coactivated neurons increase their correlation in spontaneous activity, a hallmark of ensemble formation. Coactivated neurons showed small biphasic changes in presynaptic plasticity, with an initial depression followed by a potentiation after a recovery period. Unexpectedly, optogenetic and electrical stimulation-induced significant increases in frequency and amplitude of spontaneous EPSPs, even after single-cell stimulation. In addition, we observed strong and persistent increases in neuronal excitability after stimulation, with increases in membrane resistance and reduction in spike threshold. A pharmacological agent that blocks changes in membrane resistance can revert this effect. These significant increases in excitability may partly explain the observed biphasic synaptic plasticity. We propose that cell-intrinsic changes in excitability are involved in the formation of neuronal ensembles. We propose an “iceberg” model, by which increased neuronal excitability makes subthreshold connections suprathreshold, enhancing the effect of already existing synapses, and generating a new neuronal ensemble.

Introduction

The function of the brain is anchored on the activity of groups of connected neurons, forming microcircuits (Schüz and Braitenberg, 2001; Shepherd, 2004). Specifically, groups of coactive neurons, or ensembles (also known as assemblies, synfire chains, or attractors), found in both spontaneous and evoked activity, which exhibit synchronous or correlated activity (Lorente De Nó, 1938; Hebb, 1949; Hopfield, 1982; Abeles, 1991; Cossart et al., 2003; Buzsáki, 2010; Miller et al., 2014a; Yuste, 2015; Carrillo-Reid et al., 2016, 2019; Marshel et al., 2019), could mediate memory formation (Hebb, 1949) and functional brain states (Hoshiba et al., 2017). In the cerebral cortex, these coactive states arise from reverberating patterns of multineural activity, generated by recurrent connectivity, and can occur spontaneously (Churchland and Sejnowski, 1992; Lorente de Nó, 1933). In mouse visual cortex, cortical ensembles are causally related to memory storage and percepts (Carrillo-Reid et al., 2019; Marshel et al., 2019; Miller et al., 2014). Moreover, disorganized neuronal ensembles are observed in mouse models of schizophrenia (Hamm et al., 2017).

A hypothesis of how a neuronal ensemble (i.e., a neuronal assembly) could be formed was initially proposed by Hebb in 1949. Assemblies could be formed by synaptic plasticity among coactive neurons, as a consequence of the Hebbian rule, whereby the “persistent and repeated activation of connected neurons induce metabolic changes or growth of processes in one or both cells that strengthen those connections”. One synaptic mechanism that fulfills Hebb’s rule is long-term potentiation (LTP), a long-lasting increase in synaptic efficacy after a high frequency burst electrical stimulation, and postulated to be the cellular correlate of memory and learning (Bliss and Gardner-Medwin, 1973). With LTP, increased synaptic weights enhances preferential

connectivity that leads to an increased flow of recurrent activity within ensembles (Hoshiba et al., 2017). Consistent with this, synchronous stimulation of groups of neurons 50 to 100 times, using *in vivo* two-photon optogenetics, bound them together into an "imprinted" ensemble that became spontaneously coactive after the optogenetic imprinting (Carrillo-Reid et al., 2016). However, no direct evidence has yet demonstrated that the formation of ensembles depends on changes in synaptic connections.

As an alternative hypothesis, recent experiments have revealed widespread activity-dependent cell-intrinsic mechanisms in cortical neurons, suggesting that the formation and stability of an ensemble could be due to cell-autonomous intrinsic mechanisms, such as increases in neuronal excitability (Ryan et al., 2015; Titley et al., 2017; Gill et al, 2020, Grassellil et al, 2020). This hypothesis is consistent with experiments where specific patterns of activity in the hippocampus recalls stored memories, under protein synthesis inhibitors, which should prevent LTP (Ryan et al., 2015; Tonegawa et al., 2015). Moreover, individual Purkinje cells can acquire and represent temporal pattern of inputs in a cell intrinsic manner, without synaptic plasticity (Johansson et al., 2014). Thus, ensemble consolidation could be due to changes excitability state of the neurons, instead of, or in addition to, reinforcement of its synapses (Disterhoft and Oh, 2006; Pignatelli et al., 2019).

To explore mechanisms of ensemble formation, we optogenetic and electrically stimulated neurons in mouse neocortical slices, replicating *in vitro* the optogenetic protocol to imprint ensembles *in vivo* (Carrillo-Reid et al., 2016). We then used whole-cell and perforated patch recordings, from individual neurons and pairs, to characterize electrophysiologically the stimulated neurons. We find moderate biphasic changes in synaptic properties, in the midst of

major and generalized increases in cell-intrinsic excitability, that can, at least partly, explain the synaptic changes observed. We conclude that changes in excitability play a major role in ensemble formation.

Materials and Methods

All procedures were performed by following the U.S. National Institutes of Health and Columbia University Institutional Animal Care and Use Committee guidelines (IACUC, Protocol #AC-AAAV3464). Experiments were carried out on C57BL/6 transgenic mice (Vglut1-Cre, Jackson Laboratories; RRID:IMSR_JAX:00064) and electroporated mice CD-1 (Charles River) of both sexes at postnatal 4-8 weeks-old. Animals were housed on a 12h light-dark cycle with food and water ad libitum.

Viral injection: After 1 month postnatal, animals were anesthetized with 2% isoflurane on a head-fixed stereotactic apparatus. After sterilizing the incision site, the skin was opened and, using an FG 1/4 dental drill, a small hole goes thin in the skull over the visual primary cortex (2.5 mm lateral and 0.3 mm anterior from the lambda, 200 μm from pia). We injected 300 nL of the virus at a rate of 30-40 nL/s, using a microsyringe pump (Micro 4), and a Hamilton (7653-01) glass pipette. Once the pipette was placed, we waited 5 min before and after the virus injection and closed the scalp with sutures. Viruses injected were: AAVDJ-CaMKIIa-C1V1(E162T)-TS-p2A-EYFP-WPRE (Stanford University Gene Vector and Virus Core). Mice were used for electrophysiology experiments 2–3 weeks postinjection. These mice were used only to measure evoked EPSC of optogenetically stimulated neurons.

***In utero* cortical electroporation:** Pregnant mice (CD-1, Charles River) were placed in a sterile environment following (dal Maschio et al., 2012). We performed a laparotomy, under 2% isoflurane anesthesia, and injected (0.5 mg/µL) of pCAG ChroMe-mRuby-ST (Mardinly et al., 2018), ~1µL per mouse with a glass pipette, in the left lateral ventricle of embryonic day 17 pups. After that, we placed the electrodes on the head (5 mm diameter platinum disk electrodes, (Nepa Gene #CUY650P5) to electroporate with a set of three electrical pulses for pore formation (50V; duration, 10 ms; intervals, 50ms) and then 3 electrical pulses for transferring the plasmid (8V; duration, 10 ms; interval, 50 ms). Finally, the embryos were returned to the abdominal cavity and left for their normal development until postnatal day 30.

Brain slices: Mice were anesthetized with ketamine/xylazine, after transcardial perfusion procedure and posterior cervical dislocation, to obtain brain sagittal slices as described (Ting et al., 2018). Brains were quickly dissected and cooled in a continuously gassed (95% O_2 and 5% CO_2) icy 194 Sucrose, 30 NaCl, 2.6 KCl, 26 $NaHCO_3$, 1.2 NaH_2PO4, 10 glucose, 2 $MgSO_4$, and 0.2 $CaCl_2$ Titrate pH to 7.3–7.4 with HCl. 300 µm thick sagittal slices were cut on a Leica VT1200 S vibratome (Leica Biosystems) and allowed to recover for 1 hr at 34°C aCSF solution (in mM): 195 NaCl, 2.5 KCl, 1.2 NaH_2PO_4, 26 $NaHCO_3$, 12 glucose, 1 thiourea, 1 Na-ascorbate, 1 Na-pyruvate, 2 $CaCl_2$, and 1 $MgSO_4$. Titrate pH to 7.3–7.4. Finally, slices were transferred to room temperature.

Patch-Clamp Recordings: Brain slices were carefully placed in the recording chamber on an upright microscope (Olympus, BX50WI), and continuously perfused with gassed (95% O2 and 5% CO2) aCSF at 5 ml/min. Electrophysiological recordings were performed at 30 degrees, using patch pipettes of borosilicate glass (World Precision Instruments). Pipettes were pulled with a micropipette puller (DMZ-Universal puller) to a 5 – 6 MOhm as final resistances.

For whole-cell and perforated patch-clamp, patch pipettes were filled with intracellular solution containing the following (in mM): 130 K-gluconate, 20 KCl, 10 HEPES, 10 Na_2-phosphocreatine, 4 Mg-ATP, 0.03 Na_2-GTP, and titrated to pH 7.3 with KOH. Gramicidin (sigma Aldrich) was dissolved in dimethyl sulfoxide (1mg /10 µl DMSO) and then dissolved with intracellular solution ~20 ng/ml. To allow membrane sealing, the tip of the pipette was first filled with clean solution and then the pipette was back-filled with a gramicidin-containing solution.

In each case, the patch pipettes were placed in contact with the cell with a MPC-200 micromanipulator (Sutter Instrument). Stimulation and data acquisition were sampled at 10 kHz and low pass filtered at 4kHz using a Multiclamp 700B amplifier (Molecular Devices) and Im-Patch© open-access software http://impatch.ifc.unam.mx. Recordings were discontinued when leaking current was > 25 pA or seal resistance < 1 GΩ. Recordings were analyzed with custom routines in MATLAB.

Imaging. To identify target brain region, we used an upright microscope with a 4X/0.10 NA air objective (Olympus) before switching to 60X/0.90 W NA water immersion objective to confirm ChroME or C1V1 opsin expression on target cells. For ChroME, the mRuby3 fluorescent reporter was excited with monochromatic light transmitted through a fiber optic into the microscope (Olympus 100 w high-pressure mercury burner model BH2RFLT3). Emitted fluorescence was band-passed with an Olympus U-49006 ET CY5 filter set: 620/60 excitation filter, 520 dichroic mirrors, and 700/75 emission filter. For C1V1, the EYFP fluorescent reporter was visualized via a 500/24 ex, 520 dichroic mirrors, and a 542/27 em (Semrock). Fluorescence images were acquired (50 ms exposure; 10 Hz) using a camera (Orca-ER C4742-95,

Hamamatsu) and shutter (UNIBLITZ model VCM-D1) controlled by HCImage software (Hamamatsu). We visualized individual neurons' fluorescence deep (100 μm) into the brain slice in layer 2/3, evidence of C1V1 or mRuby3 ChroMe expression.

Optogenetic stimulation. Optogenetic stimulation of ChroMe opsin was performed with a 470 nm fiber-coupled LED (M470F1, Thorlabs), fiber optic cannula (M79L01, Thorlabs), and LED driver (M00329012, Thorlabs). Optogenetic stimulation of C1V1 was performed using a 617 nm fiber-coupled LED (M617F2, Thorlabs), fiber optic cannula (CFM14L10, Thorlabs), and LED driver (DC2200, Thorlabs). The optogenetic stimulation protocol consisted of trains of 10 Hz, 5 ms light pulses for 4 s followed by a 10 s rest, we repeated the same stimulus during 15 to 80 min to mimic stimulation conditions previously used *in vivo* experiments (Carrillo-Reid et al., 2016) to co-stimulate neurons.

Only neurons that exhibited action potentials in response to each LED pulse were included in the data analysis of optogenetically stimulated neurons. LED intensity applied throughout the protocol was the lowest necessary for inducing action potentials. For optogenetically stimulated neurons, parameters were monitored before and 15 to 80 min after the stimulation protocol. Optogenetic stimulation protocol was stopped every 15 or 20 min to monitor parameters, and then restarted. For unstimulated neurons, the same parameters were monitored at the beginning and then every 15 – 20 min for 80 min approximately.

We observed that neurons expressing opsin often exhibited small alterations in intrinsic properties. Specifically, the firing rate was higher in neurons with opsins than in control cells, and the membrane resistance and membrane potential become higher and more variable than neurons without opsin expression.

Experimental design. To co-activate neurons (Carrillo-Reid et al., 2016), we delivered C1V1 or ChroME opsin in pyramidal neurons (Mardinly et al., 2018). No significant differences were found in experiments with both opsins and data were pooled together. We localized layer 2/3 pyramidal neurons in primary visual cortex of brain slices expressing opsin by virus injection and *in utero* electroporation (Figure 1A). To test whether the co-stimulation of connected neurons reinforced or created new connections (Carrillo-Reid et al., 2016), we examined pairs of connected and unconnected neurons (Figure 1B-C). We recorded and characterized evoked excitatory postsynaptic currents and potentials (EPSCs and EPSPs). We also recorded passive and active electrical properties of neurons using perforated patch-clamp recording. After measuring these parameters in control condition, we began the optogenetic or electrical stimulation protocol (Figure 1D and E). For optogenetic stimulation, action potentials were generated by trains of 10 Hz, 5 ms light pulses for 4 s followed by a 10 s rest (Figure 1D). For electrical stimulation protocol, action potentials were generated with 10 Hz trains, 5-10 ms depolarizing currents pulses 400 to 600 pA for 4 s followed by a 10 s rest (Figure 1E). During these experiments, we noticed that the time after optogenetic or electrical stimulation was important, immediately after stimulation, the membrane activity of stimulated neurons became unstable, particularly during the first 3 min after stimulation. After that, membrane potential recovered. Thus, we evaluated membrane parameters 3-5 min post-stimulation and synaptic parameters 10 min post-stimulation.

Statistical Analysis. Statistical details are showing in each figure legends. Group data are expressed as median ± sem. Wilcoxon and Mann-Whitney test were used for nonparametric analysis. Differences between two groups were considered significant when $*p < 0.05$, $**p < 0.01$ and $***p < 0.001$. All statistics were performed using statistical functions in MATLAB.

Results

Spontaneous activity becomes correlated in simultaneously stimulated neurons.

A neuronal ensemble can be defined as a group of neurons with correlated spontaneous and evoked activity (Buzsáki, 2010; Cossart et al., 2003; Ikegaya, 2004; Sasaki et al., 2007; Shepherd, 2010; Stringer et al., 2019; Yuste, 2015). Previous results have demonstrated that optogenetic coactivation of neurons can generate new ensembles *in vivo* (Carrillo-Reid et al., 2016). To explore the cellular and circuit mechanisms underlying this phenomenon, we studied the electrophysiological mechanisms that led to building of imprinted ensembles, replicating *in vitro* with the activation protocols that generates ensembles *in vivo*, optogenetic or electrical stimulation. Experiments were performed in layer 2/3 pyramidal neurons expressing the opsin ChroME in slices from primary visual cortex of adult mice of both sexes (Figure 1A).

The result of optogenetic imprinting *in vivo* was an increase in the correlation of spontaneous activity of stimulated neurons, indicative of the formation of a new ensemble (Carrillo-Reid et al., 2016). To explore if our *in vitro* stimulation protocols were effective in generating ensembles, we used paired recordings to explore whether simultaneous and repeated optogenetic or electrical activation neurons induced changes in the correlation of spontaneous activity. We recorded pairs of closely located neurons and found that 25% of recorded pairs at distances of 20 - 30 µm, were monosynaptically connected (7/28 pairs), consistent with previous reports (Markram et al., 1997; Holmgren et al., 2003; Song et al., 2005; Lefort et al., 2009; Ko et al., 2011; Levy and Reyes, 2012; Cossell et al., 2015) (Figure 1A-C). In agreement with previous studies, we found higher values of correlation of spontaneous activity between connected neuronal pairs (0.31 ± 0.16; n = 7) than between unconnected neuronal pairs (-0.04 ± 0.37; n =

21; p = 0.049 by Mann-Whitney test, Figure 1F) (Cossell et al., 2015; Ko et al., 2011; Yoshimura et al., 2005). However, ~50% (10/21) of the unconnected neuronal pairs still had relatively high correlations, comparable to connected neuronal pairs (0.32 ± 0.18; n = 9; all unconnected pairs with correlation > zero; Figure 1B). Notably, after optogenetic or electrical stimulation (Figure 1D and E), the correlation of spontaneous activity between neurons increased significantly, in both connected and unconnected pairs (0.02 ± 0.06 to 0.2 ± 0.05; n = 13 pairs, 2 connected, 11 unconnected; p = 0.049 by Wilcoxon; Figure 1G). No significant differences in correlations were found in unstimulated pairs (0.05 ± 0.1 to 0.03 ± 0.1, n = 11 pairs, p = 0.7 Wilcoxon, Figure 1H). We conclude that optogenetic and electrical stimulation increase the correlation of spontaneous activity among neurons, a hallmark of neuronal ensemble formation.

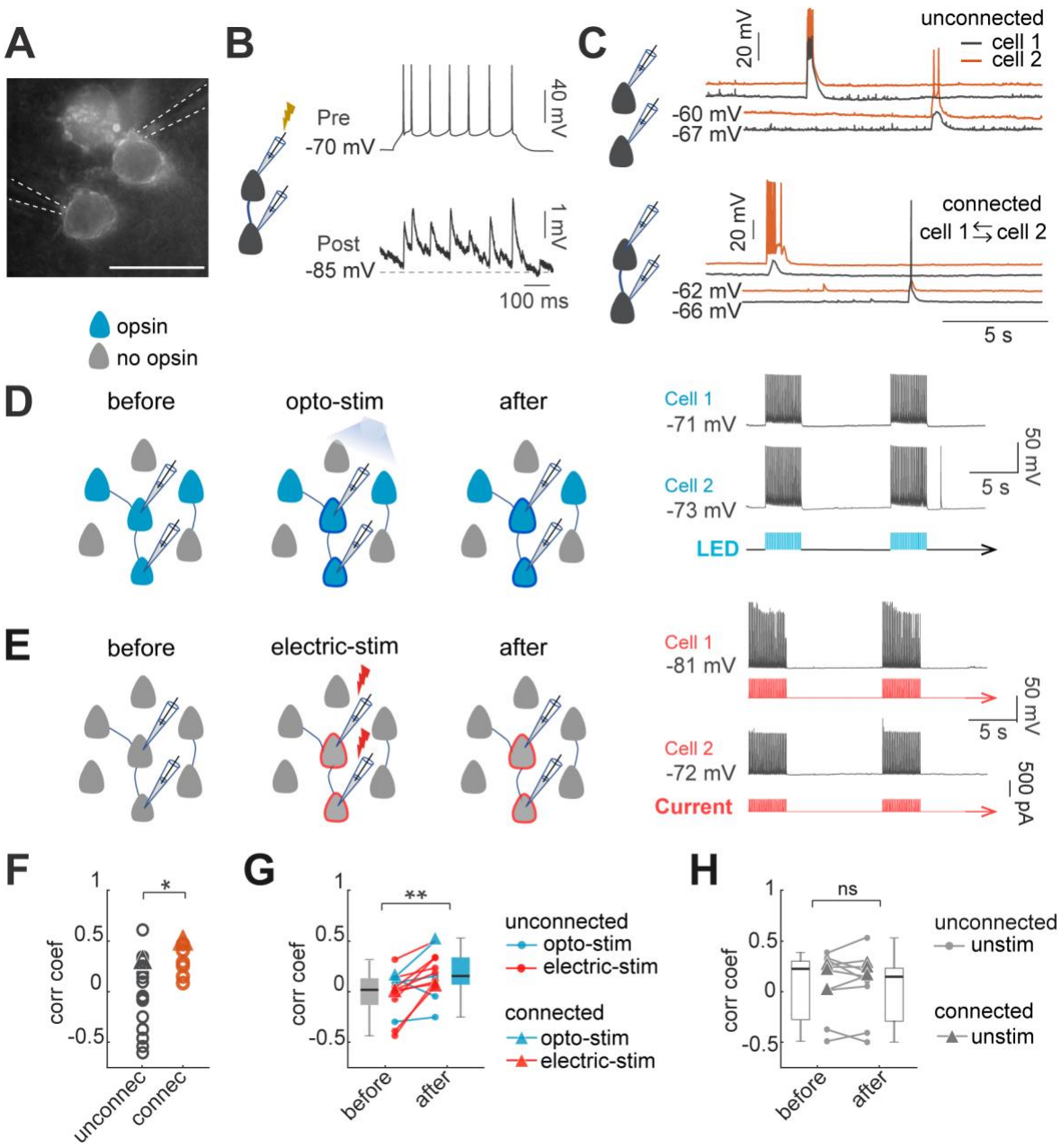

Figure 1. Optogenetic and electrical stimulation increases correlations of spontaneous activity

(**A**) Example image of Ruby3 reporter fluorescent of ST-ChroMe opsin expression in L2/3 pyramidal neurons in primary visual cortex. Brain slices were obtained from *in-utero* electroporated mice. Scale bar: 40 μM. (**B**) I*n-vitro* paired recording for evaluating monosynaptic connectivity between neurons. Perforated patch-clamp recording of presynaptic action potentials elicited by 100 pA of current injections (500 ms), followed by identification of

a monosynaptic connection, generating postsynaptic potentials time-locked to presynaptic spikes. (**C**) Spontaneous activity recording of two pairs. Top: current-clamp spontaneous activity of unconnected neurons (correlation coefficient = 0.33). Bottom: Representative paired recording from neurons that were connected bi-directionally (correlation coefficient = 0.49). (**D**) Experimental design of optogenetic stimulation protocol. Perforated current-clamp recording of two neurons with opsin expression in blue: 1 to 30 min of 10 Hz train, 5 ms light pulses for 4 s followed by 10 s of rest. (**E**) Experimental design of electrical stimulation protocol. Perforated current-clamp recording of two neurons without opsin expression in gray: 1 to 30 min of 10 Hz train, 5 ms current pulses for 4 s followed by 10 s of rest. (**F**) Correlation coefficients of connected and no connected neurons. Correlation coefficients were calculated for the first 3 minutes simultaneous recording in each pair; triangles represent correlation values of pairs showed in C. Correlation coefficients of connected (n = 7 pairs) vs. no connected (n = 21 pairs) showed significant differences p = 0.049 by Mann Whitney; 15 mice. (**G**) Correlation between pairs increased after continued co-stimulation. The graph shows increase in the correlation coefficient before and after 20 to 30 min of continuous optogenetic (blue) or electrical stimulation (red) (p = 0.004 by Wilcoxon test; n = 13 pairs, 12 mice). (**H**) Correlation before and after 20 to 30 min without stimulation (gray) (p = 0.7 by Wilcoxon; n = 11 pairs, 8 mice). Triangles in the graph represent synaptically connected pairs.

Lack of significant plasticity of synaptic currents after optogenetic stimulation

The creation of ensembles *in vivo* after optogenetic stimulation (Carrillo-Reid et al., 2016), suggested that ensembles could be built by Hebbian synaptic plasticity, by potentiation of

existing synapses of coactivated neurons. To explore this, we performed dual whole-cell and perforated patch-clamp recordings of connected neurons, and examined whether persistent and repeated optogenetic or electrical activation induced synaptic plasticity (Cossell et al., 2015; Hebb, 1949). Action potentials were induced in the presynaptic neuron with depolarizing currents (10 pulses; 400 to 600 pA, 5 ms, 20 Hz trains). For measuring synaptic currents, postsynaptic neurons were recorded in voltage-clamp, in cero current injection. We classified connections as monosynaptic if EPSC latency was 2 ± 1 ms, relative to the presynaptic spike (Figure 2A; n = 7, 5 mice). To normalize EPSC amplitudes, postsynaptic current values in the action potential start time were considered as baseline. Current values for the first EPSC ($EPSC_1$) during the stimulation trains, including failures, were averaged. A connection was defined if the average evoked $EPSC_1$ had an amplitude larger than 1.5 S.D. of the noise. Control recordings were performed with unconnected neurons (n = 21 pairs), and the optogenetic protocol did no generate any new detectable synaptic connections.

In pairs of connected neurons, we examined if optogenetic stimulation induced changes in monosynaptic currents, pooling data from whole-cell (n = 5) and perforated patch-clamp (n = 2) recordings. The average amplitude of monosynaptic ESPCs in control condition agreed with previous reports (Yoshimura et al., 2005; Feldmeyer et al., 2006; Morishima et al., 2011; Sempere-Ferràndez et al., 2019). Average $EPSC_1$ peak currents of optogenetically stimulated neurons showed no significant differences, albeit with a trend towards amplitude depression right after the stimulation, followed with a tendency towards potentiation, after a 20 minutes rest period (before: 13 ± 7 pA; after: 9 ± 7 pA; p = 0.2 Wilcoxon; 6 mice; Figure 2B, C). Control $EPSC_1$ amplitudes of unstimulated neurons also did not show significant difference before (13 ± 2 pA) and after 30 min (12 ± 2 pA; p = 0.1 Wilcoxon; n = 11, whole-cell recordings, n = 7;

perforated patch-clamp, n = 5; 6 mice). To evaluate changes in short-term plasticity, we calculated the paired-pulse ratio (PPR), i.e. the ratio of amplitudes of the second to the first EPSC in the train ($EPSC_2/EPSC_1$). We integrated data from whole-cell (n = 5) and perforated patch-clamp recordings (n = 2), and found that PPR did not significantly change with the stimulation (before: 0.95 ± 0.09 PPR; after: 0.7 ± 0.1 PPR; p = 0.4 Wilcoxon; n = 7, 5 mice; Figure 2D). Similarly, control unstimulated neurons in whole-cell (n = 5) and perforated patch-clamp recordings (n = 7) did not show significant changes in PPR before (1.08 ± 0.12) and after 30 min (1. 06 ± 0.12; p = 0.7 Wilcoxon; n = 12; 7 mice).

Biphasic plasticity of synaptic currents after electrical stimulation

We carried out similar experiments with electrical stimulation of connected pairs of neurons, thus avoiding possible side effects caused by opsin expression (see Methods) or the optogenetic stimulation of other neurons expressing opsin in the field of view. Using perforated patch-clamp, we recorded and electrically stimulated pairs of connected pyramidal neurons. After electrical stimulation, $EPSC_1$ amplitudes decreased significantly (from 14 ± 2 pA to 8 ± 1 pA; p = 0.016 by Wilcoxon; n = 7; 6 mice; Figure 2E). After pausing the stimulation for 20 min, the amplitude of evoked ESPCs recovered, with a moderate potentiation. Specifically, for electrically stimulated neurons, $EPSC_1$ amplitude recovered significantly from 8 ± 1 to 20 ± 1 pA after 20 min of post-stimulation rest (p = 0.015 by Wilcoxon; n = 7). The amplitude after the recovery period was moderately larger than the EPSCs amplitude before stimulation (14 ± 2 to 20 ± 1 pA; p = 0.015 by Wilcoxon; Figure 2E). These results are consistent with the trends found in pairs of optogenetic stimulated neurons, where $EPSC_1$ amplitude after a post-stimulation recovery period

increased from 9 ± 7 pA to 19 ± 3 pA, although no statistical comparison was possible (n = 2; Figure 2C). In contrast, control unstimulated neurons did not show a significant change (before: 13 ± 2 pA; after 30 min: 12 ± 2 pA; p = 0.6 by Wilcoxon; n = 8; 6 mice). We also measured the PPR of electrical stimulated neurons before and after electrical stimulation, finding no significant differences (before: 1.3 ± 0.15 PPR; after: 1.03 ± 0.18 PPR; p = 0.7 Wilcoxon; n = 7, 5 mice). No difference in PPR was observed before and after 20 min post-stimulation rest (1.3 ± 0.13; p = 0.1 by Wilcoxon; Figure 2E). Similarly, the PPR of unstimulated neurons did not change before (1.4 ± 0.1) and after 30 min without stimulation (1.3 ± 0.15; p = 0.5 by Wilcoxon; n = 7; 5 mice) (Figure 2F).

Biphasic plasticity of synaptic potentials after stimulation

To further explore potential postsynaptic mechanisms of ensemble formation, in a parallel set of experiments we used current-clamp to examine postsynaptic potentials (EPSPs) in connected pairs, comparing evoked EPSP amplitudes before and after optogenetic and electrical stimulation (Figure 2G). We combined data from optogenetically (n = 2, blue) and electrically-stimulated pairs (n = 7, gray). In good agreement with the voltage-clamp data, the average peak amplitude of the first EPSP ($EPSP_1$) significantly decreased after stimulation (0.43 ± 0.2 mV to 0.28 ± 0.2 mV; p = 0.004 by Wilcoxon; n = 9; 7 mice; Figure 2H). As with EPSC measurements, EPSPs recovered and became potentiated after 20 min of post-stimulation rest to 0.8 ± 0.2 mV (recovery compared with before: p = 0.008; and after stimulation: p = 0.004 by Wilcoxon). Control unstimulated neurons did not show significant differences in EPSP amplitude before (0.44 ± 0.2 mV) and after 30 min (0.42 ± 0.2 mV; p = 0.7 by Wilcoxon; n = 10; 6 mice).

In conclusion, paired recordings revealed that the coactivation of neurons generates a moderate biphasic synaptic plasticity, with an initial small depression, followed by a rebound potentiation, after several minutes of inactivity.

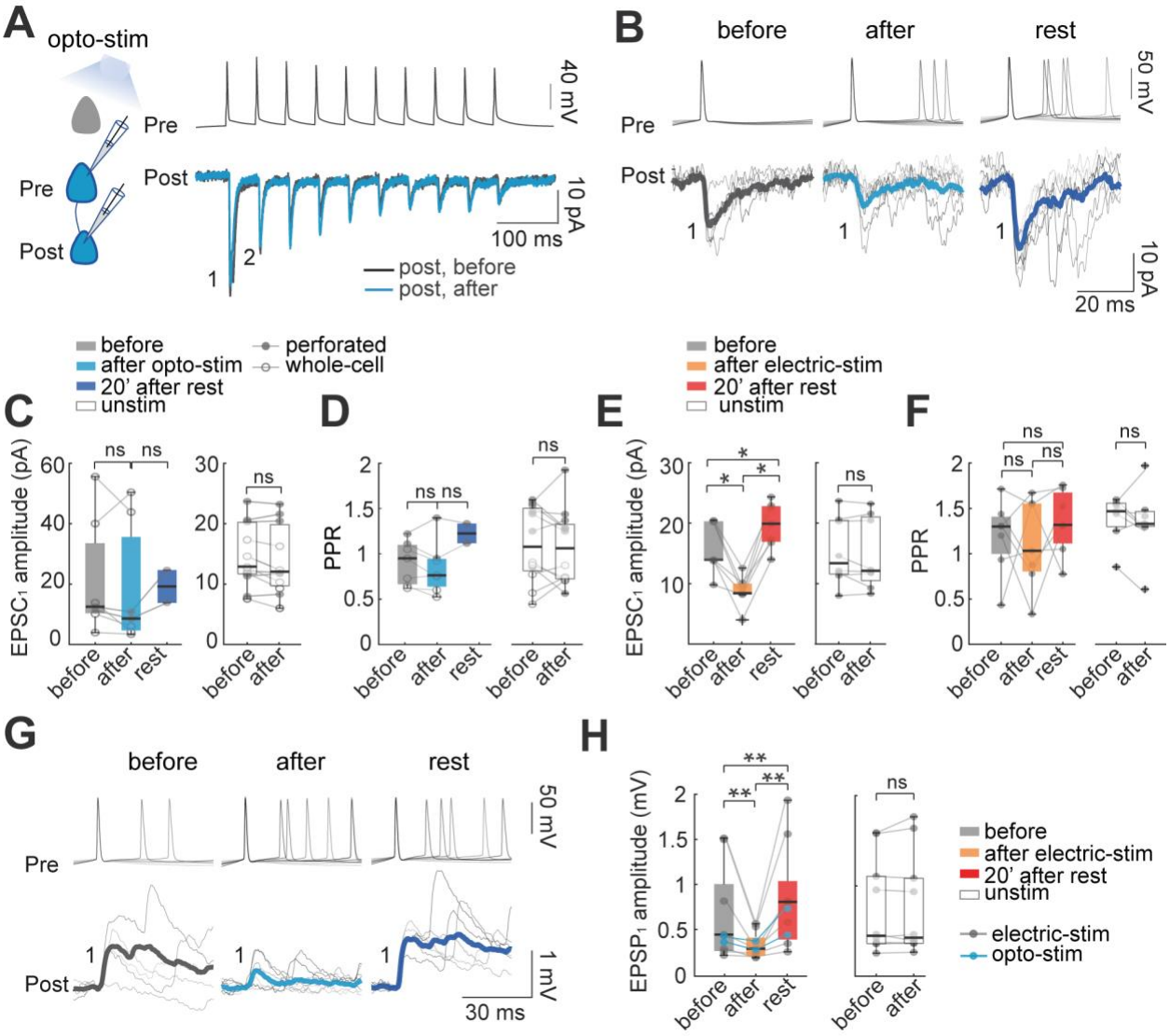

Figure 2. Effect of optogenetic and electrical stimulation in evoked EPSCs and EPSPs. (**A**) Representative paired whole-cell recording of synaptically connected neurons. Top: current-clamp recording of presynaptic action potentials in response to 10 current injections (5 ms each; 20 Hz). Bottom: voltage-clamp recording of evoked EPSC before (black) and after (blue) 30 min of optogenetic stimulation. Each trace is average of 30 successive responses evoked by

presynaptic current injection. (**B**) Representative paired recording of evoked EPSCs (perforated patch-clamp). Top: current-clamp recording of presynaptic action potentials induced by the positive current steps of the I-V curve (20 - 120 pA). Bottom: voltage-clamp recording of evoked EPSCs before and after optogenetic stimulation and after 20 min of rest post-stimulation. Thickest line is the average of successive responses to the first presynaptic action potentials for every current step of the I-V curve. (**C**) $EPSC_1$ amplitudes without significant changes before and after optogenetic stimulation. Left: mean $EPSC_1$ amplitude before and after optogenetic stimulation. Open dots correspond to whole-cell recordings, n = 5; fill dots correspond to perforated patch-clamp recordings; n = 2. Medians and blue box plot: p = 0.2 by Wilcoxon; n = 7 neurons, 5 mice). Right: Unstimulated neurons, n = 7 neurons with whole-cell and n = 5 neurons with perforated patch-clamp. Medians and white box plots; p = 0.1 by Wilcoxon; n = 12 postsynaptic neurons, 8 mice. (**D**) Comparison of mean Paired Pulse Ratio (PPR). Left: Mean PPRs before and after optogenetic stimulation and after 20 min of rest post-stimulation. PPR show no significant differences between before and after, p = 0.4; Wilcoxon; n = 7 cells, 5 mice. Right: PPR of unstimulated neurons did not show significant differences, p = 0.6 by Wilcoxon, n = 12 cells, 8 mice). (**E**) The amplitude of evoked $EPSC_1$ after electrical stimulation. Comparable to optogenetic stimulation, electrical stimulation protocol consisted of 30 min of 10 Hz train, 5 ms current pulses for 4 s followed by 10 s of rest in two neurons simultaneously, this protocol was done in brain slices without opsin expression and using only perforated patch-clamp. Left: the average $EPSC_1$ amplitude decreased after electrical stimulation (p = 0.015 by Wilcoxon; n = 7 postsynaptic neurons, 5 mice). $EPSC_1$ amplitudes were recovered with a moderate increase, after 20 min of rest post-stimulation regarding after condition (p = 0.015), and also compared to before stimulation (p = 0.015). Right: $EPSC_1$ amplitude of unstimulated neurons (p = 0.7 by

Wilcoxon; n = 8 neurons, 5 mice). (**F**) PPR remains unchanged: before and after electrical stimulation (p = 0.7 Wilcoxon; n = 8 cells, 5 mice); also, after electrical stimulation and rest post-stimulation (p = 0.2); comparison before and rest post-stimulation did not show differences either (p = 0.1), as well as PPR of unstimulated neurons; p = 0.6 by Wilcoxon, n = 12 cells, 8 mice. (**G**) Representative paired recording of evoked EPSPs (perforated patch-clamp). Top: current-clamp recording of presynaptic action potentials. Bottom: current-clamp recording of evoked EPSPs before, after optogenetic stimulation and, after 20 min of rest post-stimulation. Thickest lines are the average of the successive responses to presynaptic action potentials. (**H**) Comparison between mean $EPSP_1$ amplitude after optogenetic stimulation (blue dots; n = 2) or after electrical stimulation (gray dots; n = 7). Left: average $EPSP_1$ amplitude decreased after stimulation protocol (p = 0.004 by Wilcoxon; n = 9 neurons, 5 mice). $EPSP_1$ amplitudes were recovered with a moderate increase after 20 min of rest post-stimulation compared to after (p = 0.004 by Wilcoxon) and also, compared to before stimulation protocol (p = 0.008 by Wilcoxon). Right: $EPSP_1$ amplitude of unstimulated neurons (p = 0.7 by Wilcoxon; n = 8 postsynaptic neurons, 5 mice).

Biphasic synaptic plasticity in local circuit after optogenetic stimulation

To explore synaptic plasticity in the local circuit of optogenetically stimulated neurons, we also performed voltage-clamp and current-clamp recordings of evoked EPSCs and EPSPs in neurons *without* opsin expression but located in the same field of view (Figure 3A). Assuming a photostimulated area by the LED of 150 µM in radius, we estimated that the typical number of superficial neurons with opsin expression, and potentially activated by the light, was ~20 cells. Thus, optical stimulation could lead to a significant increase in the activity of the local circuit. To

monitor the effect of the stimulation on the local circuit, we used perforated patch-clamp from non-expressing pyramidal neurons, to measure EPSCs or EPSPs evoked by the LED, in both voltage and current-clamp. Light-evoked EPSCs or EPSPs were analyzed if the latency was >2 ms relative to LED pulse onset (Figure 3A; n = 7, 5 mice). In non-expressing cells, population light-evoked $EPSC_1$ (22 ± 3 pA) and $EPSP_1$ amplitudes (2 ± 0.1 mV) were significantly higher than unitary evoked $EPSC_1$ (14 ± 2 pA; p = 0.04 by Mann-Whitney) or $EPSP_1$ (0.43 ± 0.2 mV; p = 0.0006 by Mann-Whitney) found in connected pairs. This is likely because LED stimulated several neurons in the field simultaneously, generating a compound EPSC and EPSP.

After the optogenetic stimulation protocol (10 Hz of 5 ms pulse for 4s every 10s; 30 min), the average light-evoked $EPSC_1$ showed a significant diminution in amplitude (22 ± 3 to 11 ± 1 pA; p = 0.015 by Wilcoxon; n = 7; 6 mice; Figure 3B), and a recovery with potentiation after 20 min of rest post-stimulation (40 ± 3 pA; p = 0.015, comparing with before; p = 0.015, comparing after stimulation by Wilcoxon). Similarly, light-evoked EPSPs showed a significant decrease after 30 min optogenetic stimulation (2 ± 0.1 mV to 1.3 ± 0.2 mV; p = 0.015 by Wilcoxon; n = 7; 6 mice; Figure 3C), and also recovered with a moderate increase in amplitude after 20 min of rest post-stimulation (2.5 ± 0.3 mV; p = 0.015, comparing with before; p = 0.015, comparing with after optogenetic stimulation by Wilcoxon). These results, in excellent agreement with the connected pair data, reveals that the biphasic synaptic plasticity is also found in unstimulated neurons, thus suggesting that it is a circuit-wide phenomenon.

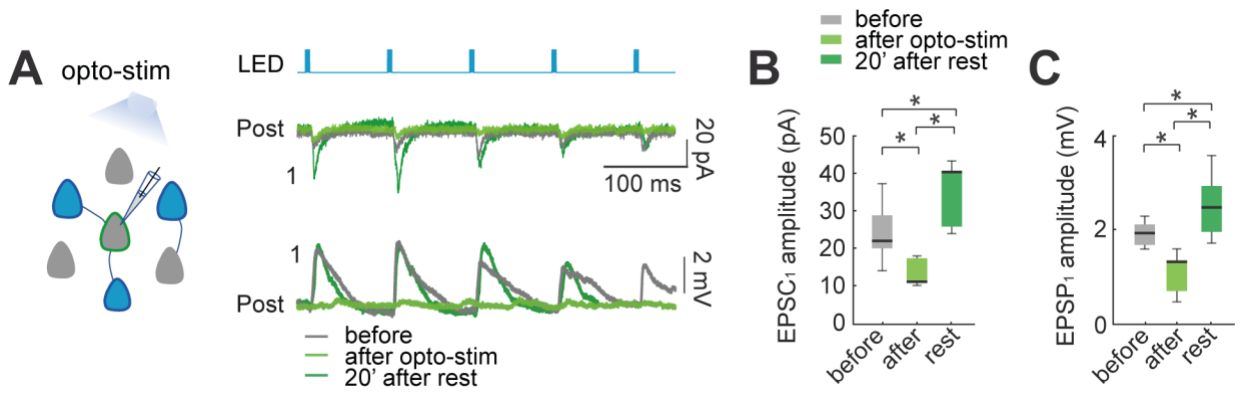

Figure 3. Effect of optogenetic stimulation in the synaptic plasticity of the local circuit

(**A**) Activation of expressing opsin neuronal population in the slice by LED pulses allowed the detection of evoked EPSCs and EPSPs in non-expressing pyramidal neurons. Voltage-clamp recording (top) and current-clamp recording (bottom) of a representative non-expressing neuron. Evoked EPSCs and EPSPs before (gray); after 30 min of optogenetic stimulation protocol (green), and 20 min post stimulation (dark green). (**B**) The amplitude of population light-evoked $EPSC_1$ (left) and (**C**) light-evoked $EPSP_1$ (right) decreased after 30 min of optogenetic stimulation ($p = 0.01$ and $p = 0.01$ respectively, by Wilcoxon; $n = 7$ postsynaptic neurons; 7 mice), they were recovered with a moderate increase after 20 min of rest ($p = 0.01$ and $p = 0.01$ respectively).

Increased of spontaneous synaptic inputs after optogenetic and electrical stimulation

To further explore the effect of the optogenetic and electrical stimulation on population activity, we measured spontaneous EPSP from recorded neurons, and compared them before and after stimulation (Figure 4A). To measure spontaneous EPSPs, we low-pass filtered current-clamp recordings, subtracting membrane potential oscillations, to obtain comparable baselines of EPSP amplitudes (Juárez-Vidales et al., 2021). We detected EPSPs with amplitudes between 0.3 mV

and 10 mV and analyzed changes in the frequency of spontaneous EPSP before and after optogenetic stimulation (Figure 4A-B). The frequency of spontaneous EPSP significant increased from 90 ± 9 EPSPs/min before to 127 ± 19 after optogenetic stimulation ($p = 0.004$ by Wilcoxon; $n = 10$; 5 mice) (Figure 4D left). We also observed increases in EPSP amplitude (0.38 ± 0.01 to 0.41 ± 0.02 mV; $p = 0.04$) (Figure 4E left). In control recordings (Figure 4D-E right), non-expressing pyramidal neurons showed no statistically differences in the frequency of spontaneous EPSPs (93 ± 25 to 64 ± 18; $p = 0.06$), or in EPSP amplitude (0.37 ± 0.004 to 0.37 ± 0.004 mV; $p = 0.5$; $n = 11$; 8 mice).

Similarly, electrical stimulated neurons showed a significant increase in the frequency of spontaneous EPSPs from 80 ± 12 to 118 ± 17 EPSPs/min ($p = 0.001$ by Wilcoxon; $n = 13$; 8 mice) and EPSP amplitude (0.37 ± 0.03 to 0.40 ± 0.03 mV; $p = 0.03$) (Figure 3F-G left). In unstimulated neurons (Figure 3F-G right), we found no statistically difference in the frequency of spontaneous EPSPs (98 ± 18 to 93 ± 15; $p = 0.4$), or any significant differences in EPSP amplitude (0.37 ± 0.01 to 0.38 ± 0.01 mV; $p = 0.4$; $n = 11$; 8 mice).

These results reveal major changes in spontaneous synaptic inputs after optogenetic and electrical stimulation. The increase in spontaneous EPSPs amplitude could partly explain their increased frequencies, as smaller EPSPs will become detectable. Importantly, since increases in spontaneous EPSP frequency and amplitude also occur even after electrical stimulation of individual neurons, our results demonstrate that neurons become more sensitive to synaptic inputs after stimulation, in a cell intrinsic manner.

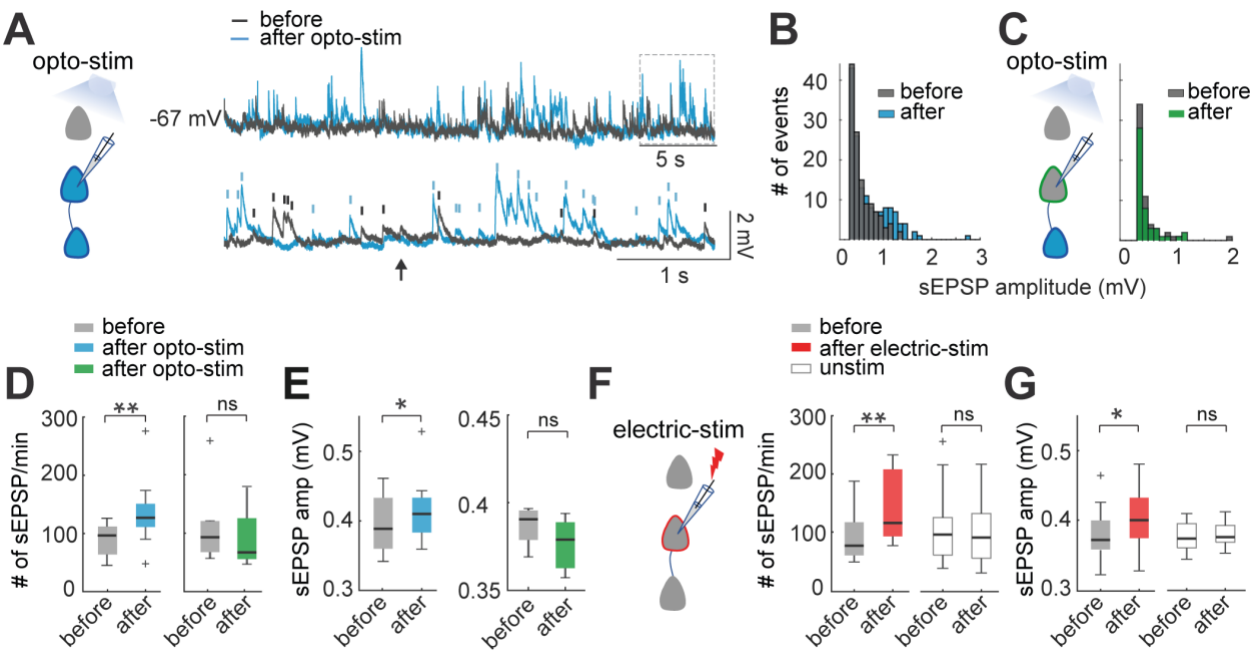

Figure 4. Optogenetic and electrical stimulation amplifies spontaneous EPSPs.

(**A**) Representative perforated patch-clamp recording of a neuron in current-clamp. Top: spontaneous EPSPs of a neuron before and after optogenetic stimulation protocol. Bottom: Section in the top trace shows spontaneous EPSPs amplitude > 0.3 mV that was identified before (gray) and after (blue) optogenetic stimulation protocol in a one-minute recording. Arrow shows a tentative EPSP < 0.3 mV that was not detected by the threshold (0.3 mV). (**B**) Frequency histogram of spontaneous EPSPs amplitudes shows that after optogenetic stimulation, the number of events increased as well as the number of events with higher amplitudes. (**C**) Frequency histogram of spontaneous EPSPs amplitudes shows that the number of events of a non-expressing pyramidal neuron remained unchanged before and after optogenetic stimulation of expressing neuronal population. (**D**) The number of spontaneous EPSPs increased in optogenetically stimulated neurons but not in non-expressing neurons. Left: Optogenetic stimulation of neurons: blue median and box plot; p = 0.004 by Wilcoxon; 8 mice. Right: Number of spontaneous EPSPs of non-expressing pyramidal neurons before and after

optogenetic stimulation protocol: green median and box plot; p = 0.06 by Wilcoxon; 5 mice. (**E**) The amplitude of spontaneous EPSPs increased in optogenetically stimulated neurons but not in non-expressing neurons. Right: Optogenetic stimulated neurons: blue median and box plot; p = 0.04 by Wilcoxon. Left: Non-expressing neurons: green median and box plot; p = 0.5 by Wilcoxon. (**F**) The number of spontaneous EPSPs increased after electrical stimulation. Electrical stimulated neurons: red medians and box plot; p = 0.0012 by Wilcoxon; 9 mice. Unstimulated neurons: white medians and box plot; p = 0.4 by Wilcoxon; 9 mice. (**G**) The amplitude of spontaneous EPSPs increased after electrical stimulation. Electrical stimulated neurons: red median and box plot; p = 0.003 by Wilcoxon. Unstimulated neurons: white medians and box plots; p = 0.4 by Wilcoxon.

Optogenetic stimulation increases neuronal excitability

Our results demonstrated that optogenetic and electrical stimulation, even of individual neurons, could induce changes in intrinsic membrane properties, or cellular excitability. This is in agreement with an extensive literature that has described non-synaptic cellular plasticity in a variety of experimental preparations (Abraham et al., 2019; Malik and Chattarji, 2012; Marder and Goaillard, 2006; Paz et al., 2009; Ryan et al., 2015; Titley et al., 2017; Xu, 2005; Yang and Santamaria, 2016). To explore these mechanisms, we evaluated active and passive intrinsic electrophysiological parameters such as current injection-dependent firing, frequency, membrane resistance, membrane potential, and firing threshold. We recorded individual neurons with perforated patch-clamp before and after optogenetic and electrical stimulation (Figure 5).

We first measured membrane potential dependency to current injections with I-V plots in pyramidal neurons with opsin expression. To do this, we kept the membrane potential at -70 mV

and applied series of 500 ms current injections ranging from -100 pA to 160 pA, with 20 pA alternating positive and negative steps (black traces; Fig. 5A). We first observed a significant increase in the evoked number of spikes after optogenetic stimulation (blue traces; 5 ± 1 and 6 ± 1 spikes; p = 0.015 by Wilcoxon; n = 12; 8 mice; Figure 5D-a). These increases in the firing rate were not observed in unstimulated neurons (5 ± 1 and 5 ± 1; p = 1 by Wilcoxon; n = 7; 6 mice; Figure 5D-b). We also noticed that neurons expressing opsin exhibited a small alteration in their intrinsic properties. In particular, the firing rate became higher than the neurons without opsins in control condition (5 ± 1 firing rate of neurons with opsin expression, 3.5 ± 1 neurons without opsin, but this difference was not significant p = 0.1 by Mann-Whitney; n = 7; 6 mice).

Neurons needed at least 15 - 20 min of optogenetic or electrical stimulation to increase their excitability, but, after their firing rate increased, it was stable for the 80 min duration of the experiment (6 ± 1 to 6 ± 1 spikes; p = 0.5 by Wilcoxon; n = 7; 5 mice; Figure 5B). The long-lasting increase in firing rate did not require continued stimulation, since after pausing optogenetic stimulation for 30 min, it remained elevated (6 ± 1 to 6 ± 1 spikes; p = 0.8 by Wilcoxon; n = 7; 5 mice; Figure 5C). Similar results were found for the average instantaneous firing frequency, which increased after optogenetic stimulation (from 15 ± 3 to 17 ± 3 Hz; p = 0.015 by Wilcoxon; n = 12; 8 mice; Figure 5E-a. Unstimulated neurons did not show significant differences (from 16 ± 3 to 16 ± 3 Hz; p = 0.5 by Wilcoxon; n = 7; 5 mice; Figure 5E-b). Finally, to evaluate the modification of firing properties that could facilitate burst induction, we measured the mean frequency of the two first spikes for each current step, finding a significant increase (before: 24 ± 3 Hz; after optogenetic stimulation: 27 ± 3 Hz; p = 0.015 Wilcoxon; Figure 5F-a), whereas unstimulated neurons did not show significant differences after 30 minutes of recordings (25 ± 6 and 24 ± 6 Hz; p = 0.2 by Wilcoxon; n = 7; 5 mice; Figure 5F-b). To rule out that these

changes in firing properties were due to the illumination, we recorded neurons without opsin expression in perforated patch-clamp, before and after optogenetic stimulation. We did not detect any significant change in current injection firing-dependence (4 ± 1 and 4 ± 1 spikes; p = 1, by Wilcoxon; n = 7; 5 mice), nor in the average instantaneous frequency (7 ± 2 Hz before; and 7 ± 2 Hz after; p = 0.6 by Wilcoxon). These data, similar to those from unstimulated neurons, demonstrate that the LED illumination does not induce changes in cellular excitability.

Terfenadine reverts optogenetic stimulation increases neuronal excitability

These results revealed that optogenetic stimulation produced a robust increase in current-dependent firing. To pharmacologically explore potential mechanisms underlying these changes, we used terfenadine, a pharmacological agent that blocks currents mediated by Ether-a-go-go Related Gene (ERG) channels, and, in neocortical pyramidal cells, prevents persistent firing and increases in membrane resistance (Cui and Strowbridge, 2018). Indeed, the increases in firing rate and frequencies induced by optogenetic stimulation reverted to control conditions after the application of 10µM terfenadine (5 ± 1 and 4 ± 1 spikes; p = 0.015 by Wilcoxon; n = 7; 5 mice; Figure 5D-c). No differences were found comparing with before stimulation and when terfenadine was applied (4 ± 1 and 4 ± 1 spikes; p = 0.06 by Wilcoxon; n = 7; 5 mice). However, in unstimulated neurons without opsin, terfenadine generated a reduction in firing rate (4 ± 1 before; and 3 ± 1 terfenadine p = 0.03 by Wilcoxon; n = 7; 5 mice). We concluded the increase in excitability due to optogenetic stimulation can be reverted by terfenadine. This could be due to blockage of baseline conductances, such as ERG channels or other targets like histamine1, kir 6, and Kv11.1 (Carter et al., 1985).

Electrical stimulation increases neuronal excitability

After characterizing studying the changes in firing properties due to optogenetic activation, we explored if single-cell electrical stimulation generated similar alterations. Electrical stimulation via a patch pipette avoids possible side effects produced by the optogenetic stimulation, or by the activation of an undetermined number of opsin-expressing neurons. Electrical stimulation of one neuron at the time also rules out synaptic effects. In these single cell electrical stimulation experiments, we observed similar effects as in optogenetic stimulation: increases in firing rate (before 4 ± 1 spikes; after 5 ± 1 spikes; $p = 0.015$ by Wilcoxon; $n = 22$; 12 mice; Figure 5D-d); increases in average frequency (8 ± 2 Hz before; 10 ± 2 Hz after; $p = 0.015$ by Wilcoxon; Figure 5E-d); and increases in frequency of the first two spikes (14 ± 3 Hz before; 17 ± 3 Hz after; $p = 0.015$ by Wilcoxon; Figure 5F-d). Unstimulated neurons did not show any changes in firing rate (before 4 ± 1; after 4 ± 1 spikes; $p = 1$ by Wilcoxon; $n = 10$; 8 mice; Figure 5D-e); or average frequency (9 ± 2 Hz before; and 9 ± 2 Hz after; $p = 0.015$ by Wilcoxon; Figure 5E-e); nor in the first frequency (15 ± 3 Hz before; and 15 ± 3 Hz after; $p = 1$ by Wilcoxon; Figure 5F-e).

The consistency in results from optogenetic and electrical stimulation indicate that the increases in cellular excitability are not due to opsin expression or optogenetic protocol, and is a property of individual neurons that can be induced by stimulation of individual cells.

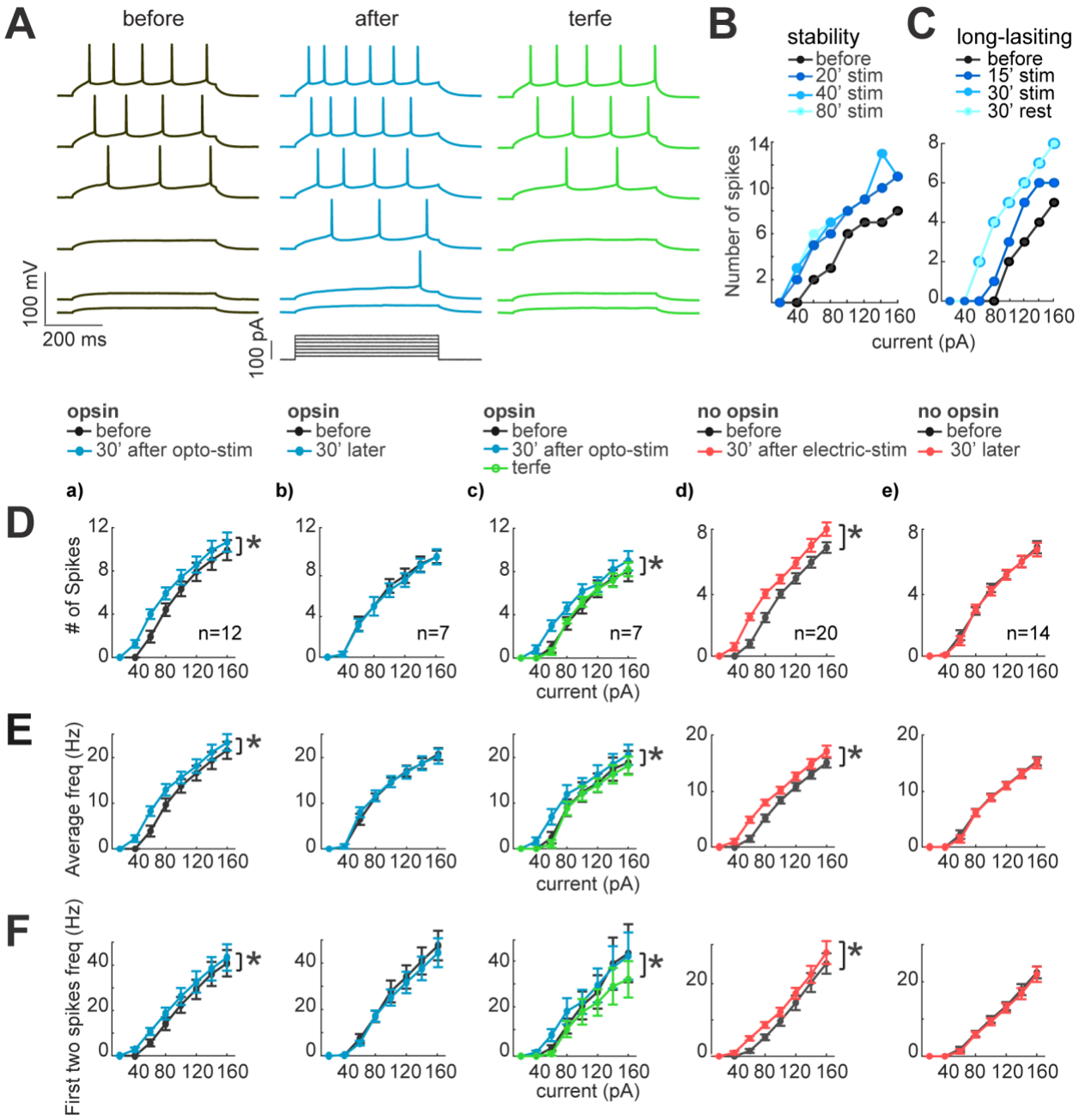

Figure 5. Neuronal excitability increases after optogenetic or electrical stimulation.

(**A**) Current dependence firing rate increases after optogenetic or electrical stimulation protocol. This returns to basal conditions after the application of terfenadine. Representative membrane voltage recordings with perforated patch-clamp (top) in response to 500 ms series of 20 pA

current steps (20 to 120 pA, bottom). Black traces show membrane potential in response to current steps before stimulation. Blue traces represent membrane voltage recordings of neurons with opsin expression and responses after 30 min of optogenetic stimulation. The green traces show the effect of the terfenadine (10 µM) in the membrane potential post-stimulation. (**B**) Decrease in the rheobase after stimulation is stable. Current-dependent firing rate increased in a representative neuron after 20 min of continuous optogenetic stimulation. This firing rate did show more changes even after 80 min of continued stimulation ($p = 0.4$ by Wilcoxon; $n = 7$ neurons, 5 mice). (**C**) Decrease in the rheobase after stimulation is long-lasting. Gradual increase in the firing rate of a representative neuron after 15 min of optogenetic stimulation and then after 30 min. 30 min post-stimulation (rest), the neurons kept their membrane excitability increased ($p = 0.4$ by Wilcoxon; $n = 7$ neurons, 5 mice). (**D**) Neuronal activity increase after optogenetic or electrical stimulation. For every graph (a - e), the thicker black lines are average spikes of all neurons before stimulation protocol. Thicker lines color for the average spikes correspond to a) blue, optogenetic stimulation; b) blue, 30 minutes without stimulation in neurons with opsin expression; c) green, terfenadine (10µM) effect after optogenetic stimulation; d) red, electrical stimulation in neurons without opsin expression; e) red, 30 minutes without stimulation in neurons without opsin expression. Data represent mean ± SEM. *$p < 0.05$ by Wilcoxon. (**E**) Same as **D** but for average frequency for each current step. *$p < 0.05$ by Wilcoxon. (**F**) The frequency of the first two action potentials increased for the lower current steps after stimulation. Same as **D** but for the average of the first two action potentials frequency. *$p < 0.05$ by Wilcoxon.

Optogenetic and electrical stimulation increase membrane resistance

An increase in excitability could be due to an increase in membrane resistance (Marder and Goaillard, 2006). To calculate membrane resistance, we measured membrane potential changes produced by hyperpolarizing current pulses of low intensity (from 40 to -100 pA; 500 ms duration, applied every second), before and after optogenetic stimulation (Figure 6A). Membrane input resistance was measured from the voltage-current (I-V) relationship (Figure 6B). We observed a significant increase in input resistance from 278 ± 18 mΩ before to 305 ± 22 mΩ after optogenetic stimulation ($p = 0.0001$ by Wilcoxon; $n = 14$; 8 mice; Figure 6C-a). Meanwhile, resistances of unstimulated neurons, with opsin expression, did not show any change before (318 ± 23 mΩ) and 30 minutes after (309 ± 24 mΩ; $p = 0.9$ by Wilcoxon; $n = 8$; 8 mice, Figure 6C-b). These increases were reverted by the addition of terfenadine (from 172 ± 15 mΩ after stimulation to 153 ± 16 mΩ after terfenadine; $p = 0.02$ by Wilcoxon; $n = 9$; 7 mice; Figure 6C-c). Also, the addition of terfenadine brought back the resistance to its pre-stimulation values, 158 ± 15 mΩ before stimulation to 153 ± 16 mΩ with terfenadine; $p = 0.9$ by Wilcoxon. Furthermore, electrical stimulation in non-expressing neurons also induced a significant increase in the input resistance (from 176 ± 9 to 185 ± 9 mΩ; $p = 0.0003$ by Wilcoxon; $n = 10$; 8 mice; Figure 6C-d). Unstimulated neurons did not display changes in membrane resistance (before 171 ± 11 to after 174 ± 8 mΩ; $p = 0.3$ by Wilcoxon; $n = 10$; 8 mice; Figure 6C-e). Control experiment with non-expressing neurons did not show any alteration in membrane resistance after optogenetic stimulation of the slices (before 176 ± 20 mΩ; after 179 ± 20 mΩ; $p = 0.3$ by Wilcoxon).

It has been reported that membrane resting potential can also change through increases in excitability, resulting in depolarization (Debanne et al., 2019; Mellor, 2002; Ross and Soltesz, 2001). To explore this, we calculated membrane resting potential as the median of spontaneous

membrane activity with zero current injection. We observed that membrane resting potential remained stable under all condition: before and after optogenetic stimulation (-73 ± 2 to -72 ± 1 mV; p = 0.4 by Wilcoxon; n = 10; Figure 6D-a); unstimulated neurons (-73 ± 2 to -75 ± 2 mV; p = 0.8 by Wilcoxon; n = 13; Figure 6D-b). The application of terfenadine after stimulation also did not reveal significant changes in membrane potential (-78 ± 2 to -77 ± 2 mV; p = 0.8 by Wilcoxon; n = 8; Figure 6D-c) and no changes before and after electrical stimulation (-80 ± 1 to -79 ± 1 mV; p = 0.9 by Wilcoxon; n = 13; Figure 6D-d). This lack of resting membrane potential changes during intrinsic neuronal excitability agrees with previous reports (Cudmore and Turrigiano, 2004; Disterhoft et al., 1986; Pignatelli et al., 2019). We conclude that the increase in excitability induced by optogenetic or electrical stimulation is associated with increases in membrane resistance but not with membrane potential depolarization.

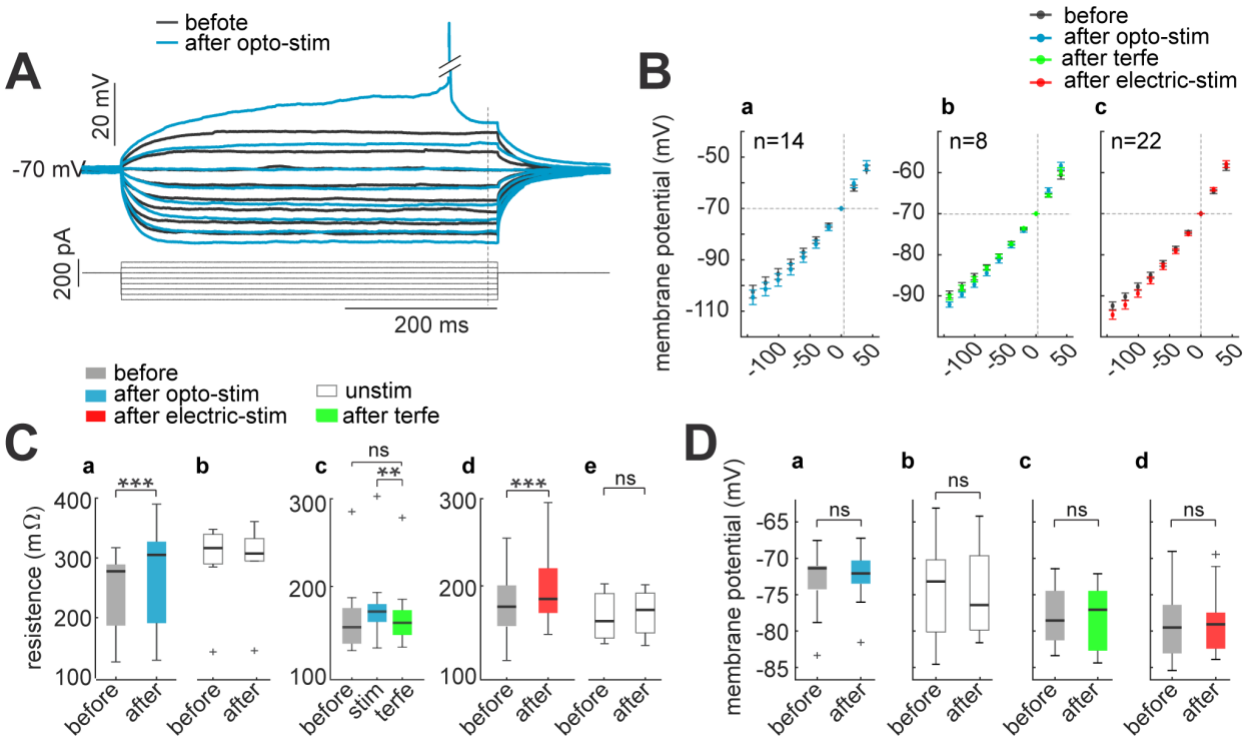

Figure 6. Membrane input resistance increases after optogenetic or electrical stimulation

(**A**) Membrane resistance increases after optogenetic or electrical stimulation; these returns to control condition after terfenadine application. Representative membrane voltage recordings with perforated patch-clamp in response 500 ms series of 20 pA current pulses from 40 to -100 pA (bottom). Black traces show membrane potential dependence before optogenetic stimulation, and blue traces correspond to 30 min after (**B**) I-V plots show the relation between current injection and the membrane potential (Ohm's law: Resistance = V/I). For every graph (a - c), black dots are the average voltage membrane response to current steps before the stimulation protocol. Blue average voltage membrane corresponds to a) optogenetic stimulation; b) green, the effect of terfenadine (10µM) after optogenetic stimulation; c) red, electrical stimulation in neurons without opsin expression. Data represent mean ± SEM. (**C**) Membrane resistance increased after optogenetic or electrical stimulation. a) Optogenetic stimulated neurons: median and blue box plot; p = 0.0001 by Wilcoxon; n = 14 neurons, 9 mice. b) Unstimulated neurons with opsin expression: median and gray box plots; p = 0.7 by Wilcoxon, n = 8 neurons, 5 mice. c) Terfenadine (10µM) effect after optogenetic stimulation: median and green box plot; p = 0.003 by Wilcoxon; n = 8 neurons, 5 mice. d) Electrical stimulated neurons: median and red box plot; p = 0.00004 by Wilcoxon; n = 22 neurons, 15 mice. e) Unstimulated neurons without opsin expression: median and gray box plot; p = 0.5 by Wilcoxon; n = 11 neurons, 8 mice. (**D**) Resting membrane potential remain without changes after stimulation. a) Optogenetic stimulated neurons: median and blue box plot; p = 0.4 by Wilcoxon; n = 10 neurons. b) Unstimulated neurons: median and gray box plots; p = 0.8 by Wilcoxon; n = 13 neurons. c) Terfenadine (10µM) effect after stimulation: median and green box plot; p = 0.8 by Wilcoxon; n = 8 neurons. d) Electrical stimulated neurons: median and red box plot; p = 0.9 by Wilcoxon; n = 13.

Lowering of action potential threshold after optogenetic and electrical stimulation

The changes in frequencies of the first two spikes that we observed could also be due to changes spike threshold. Burst firing depends on the interplay between the afterhyperpolarization (AHPs) and afterdepolarizations (ADPs) that follow the first action potential (Brumberg et al., 2000; Mahon and Charpier, 2012; Paz et al., 2009). To explore this, we evaluated the dynamics of action potentials using phase plot analysis. We used the first spikes from 60 pA current injections in the I-V dataset; because during this current step, most neurons consistently displayed action potentials before and after optogenetic or electrical stimulation protocol. Action potentials were detected after setting a threshold of >0.00015 in the first derivative of membrane potential waveform, a value that corresponds to the firing threshold, and voltage/time values (mV/ms) were plotted as a function of membrane potential (mV). In this analysis, action potentials are represented as a loop in which the starting point represents the firing threshold (Figure 7A). After optogenetic stimulation, the majority of phase plots displayed a leftward offset, making evident a lowering in firing threshold (-41± 1 before to -43.7 ± 1 mV after; $p = 0.0012$ by Wilcoxon; $n = 13$, 8 mice; Figure 7B-a). This change was partially reverted by terfenadine (10 µM; -45 ± 1 mV after stimulation to -44 ± 1 mV after terfenadine; $p = 0.05$ by Wilcoxon; $n = 8$, 6 mice; Figure 7B-c). We found no statistically significant differences in firing threshold of unstimulated neurons, when comparing the beginning and the end of the recording (-41 ± 2 and -41 ± 2 mV respectively; $p = 0.7$ by Wilcoxon; $n = 8$ cells, 5 mice; Figure 7B-b). Also, non-expressing neurons did not show any alteration of firing threshold after optogenetic stimulation of the slices (before -40 ± 1.4 mV to -40 ± 1.5 mV after; $p = 0.7$ by Wilcoxon). Thus, the LED light did not induce damage or alterations in this cell-intrinsic parameter.

We also documented a similar lowering of the threshold voltage in electrically stimulated neurons (before -42 ± 0.8 mV; after 44 ± 0.8 mV; p = 0.00004 by Wilcoxon; n = 22 cells; Figure 7B-d). Unstimulated neurons displayed no changes in threshold voltage (-42 ± 0.7 mV at the first min and -43 ± 0.8 mV 30 min later; p = 0.5 by Wilcoxon; n = 11, 8 mice; Figure 7B-e).

The combine increase in membrane resistance and reduction of firing threshold, can explain the increase in neuronal excitability previously observed. Thus, optogenetic and electrical stimulation significantly increases action potential firing in response to similar synaptic inputs, facilitating the formation of a neuronal ensemble.

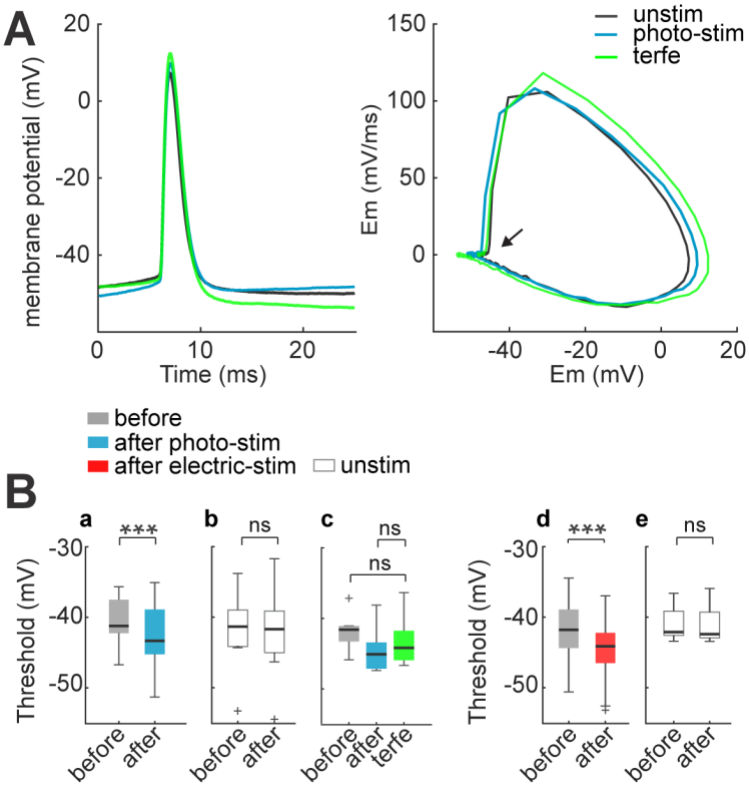

Figure 7. Spike threshold decreases after optogenetic and electrical stimulation

(A) Firing threshold shifts to more negative potentials after optogenetic and electrical stimulation. Left: the firing threshold was taken to the first action potential generated with 60 pA

current step: before (black), after 30 min of optogenetic stimulation (blue) and, terfenadine post-stimulation (green). Right: phase plot of action potentials: before (black), after (blue), and terfenadine (green). The arrow shows the firing threshold position. (**B**) Firing threshold was detected for every cell before and after: a) optogenetic stimulation, median and blue box plot ($p = 0.0009$ by Wilcoxon, $n = 14$ cells, 9 mice); b) Unstimulated neurons with opsin expression, median and gray box plots ($p = 0.7$ by Wilcoxon; $n = 8$ cells, 5 mice). c) Terfenadine (10µM) post-stimulation, median and green box plot; $p = 0.003$ by Wilcoxon; $n = 8$ neurons, 5 mice; firing threshold before stimulation and after terfenadine ($p = 0.1$ by Wilcoxon); d) electrical stimulation, median and red box plot ($p = 0.00004$ by Wilcoxon; $n = 22$ cells, 15 mice). e) Unstimulated neurons without opsin, median and gray box plot ($p = 0.7$ by Wilcoxon; $n = 11$ cells, 8 mice).

Discussion

The traditional view of how a neuronal ensemble (i.e., an assembly) is created is by strengthening its synaptic connections after repeated coactivation (Bliss and Lømo, 1973; Carrillo-Reid et al., 2016; Cossell et al., 2015; Hebb, 1949; Hoshiba et al., 2017). However, several reports have questioned whether synaptic plasticity is the only mechanism of circuit plasticity, proposing instead cell-intrinsic mechanisms (Angelo et al., 2012; Brown et al., 2019; Disterhoft and Oh, 2006; Marder and Goaillard, 2006; Ryan et al., 2015; Zhang and Linden, 2003). Consistent with this, an in contradiction with our predictions that synaptic plasticity mediates neuronal ensembles (Carrillo-Reid et al, 2016), we describe that simultaneous optogenetic or electrical stimulation of neurons *in vitro* increases the excitability of the stimulated cells. Our experimental procedures, similar to those that build ("imprint") neuronal

ensembles *in vivo* (Carrillo-Reid et al., 2016), lead to increases in correlations of spontaneous activity, a hallmark of a neuronal ensemble, just as it does *in vivo*. The cellular and/or synaptic mechanism induced by this optogenetic and electrical activation could contribute to neuronal ensemble development (Penn and Shatz, 1999; Zhang and Poo, 2001), flexibility and plasticity (Clopath et al., 2017; Kirkwood et al., 1996; Mrsic-Flogel et al., 2007; Pérez-Ortega et al., 2021; Wandell and Smirnakis, 2009; Wiesel and Hubel, 1963).

Role of synaptic mechanisms in ensemble formation

Our stimulation protocols induced a moderate biphasic plasticity of connected neurons and also in the local circuit, with an initial depression followed by a recovery potentiation. This agrees with reports that EPSP amplitude can decrease after high stimulation frequencies, but recovers from depression by using lower stimulation rates (Feldmeyer et al., 2006). This is consistent with the hypothesis that persistent optogenetic or electrical stimulation reduces the readily releasable pool of synaptic vesicles in the presynaptic neuron inducing, first, synaptic depression and, after a period of rest, a rebound which is revealed as a potentiation (Feldmeyer et al., 2006; Schneggenburger et al., 2002). But, in addition to these synaptic changes, our results demonstrate that persistent and simultaneous stimulation robustly increases membrane resistance. Thus, neuronal excitability could increase the efficiency of existing synaptic connections between neurons in an ensemble, without significant short-term or long-term synaptic plasticity.

Our results appear in contradiction with the hypothesis that the formation of an ensemble is due to increases in synaptic connectivity of synchronous neurons (Hebb, 1949; Cossell et al., 2015; Hoshiba et al., 2017). Consistent with this hypothesis, there is preferential connectivity between neurons with similar receptive fields (Cossell et al., 2015; Ko et al., 2011; Yoshimura et al.,

2005). Increased synaptic connectivity also probably underlies pattern completion in cortical ensembles (Carrillo-Reid et al., 2019; Pignatelli et al., 2019), and a few strong connections could drive local excitation of the majority of neurons with weak connectivity (Cossell et al., 2015; Holmgren et al., 2003; Ko et al., 2011; Lefort et al., 2009; Levy and Reyes, 2012; Markram et al., 1997; Song et al., 2005). Based on previous studies, we expected to observe synaptic efficiency changes (Bliss and Gardner-Medwin, 1973) between connected neurons after ensemble formation. Using paired recordings, we find similar rates of connectivity between neuronal pairs as previous reports (Cossell et al., 2015; Holmgren et al., 2003; Ko et al., 2011; Lefort et al., 2009; Levy and Reyes, 2012; Markram et al., 1997; Song et al., 2005). And, also consistent with many reports, connected neurons display higher correlation in spontaneous activity than unconnected ones (Cossell et al., 2015; Ko et al., 2011; Yoshimura et al., 2005). Interestingly, our results also showed that 50% of unconnected neurons can be as correlated as connected neurons. However, contrary to our own expectations, we did not detect any new connections formed after optogenetic stimulation previously unconnected neurons. Moreover, rather than synaptic potentiation, we found depression of evoked EPSCs and EPSPs. Although also detect a moderate potentiation after 20 min of rest, and we cannot rule out that Hebbian synaptic plasticity contributes to this potentiation, it is possible that this could instead be due to a recovery of the ready releasable pool, together with increased synaptic efficacy due to changes in postsynaptic and presynaptic excitability. Indeed, we find that spontaneous EPSPs and EPSCs become amplified in electrically stimulated neurons. A larger synaptic input could also naturally result from an overall increase in neuronal firing too, since increased neuronal excitability would result in increase in neurotransmitter release. This agrees with reports that reveal that synaptic inputs can be enhanced by intrinsic membrane mechanisms (Hu et al., 2002; Li et al., 2020;

Manabe et al., 1992; Marder and Goaillard, 2006; Narayanan and Johnston, 2008; Turrigiano et al., 1998). For all these reasons, we suspect synaptic plasticity can be explained by the effects of the stimulation protocols in the ready releasable pool and intrinsic changes in excitability in the stimulated neurons and the network.

Role of intrinsic mechanisms in ensemble formation

Changes in intrinsic properties are known to modulate EPSP amplitude, for example, by the modification of membrane conductance induced by postsynaptic stimulation (Hu et al., 2002; Li et al., 2020; Manabe et al., 1992; Marder and Goaillard, 2006; Narayanan and Johnston, 2008; Turrigiano et al., 1998). These changes might be due to modification in intrinsic membrane conductances (Li et al., 2020; Manabe et al., 1992; Narayanan and Johnston, 2008), and they could amplify synaptic inputs and improve the accuracy of synaptic integration of neurons (Desai et al., 1999; Mahon and Charpier, 2012; Malik and Chattarji, 2012; Sjöström et al., 2008; Turrigiano et al., 1994).

Confirming the importance of intrinsic mechanisms, in our experiments, robust increases in firing rate were easily detected in optogenetic and electrically stimulated neurons. Even though we have noticed that the expression of opsin by itself can have small effects in excitability, opsin-expressing neurons still had major changes in intrinsic properties after optogenetic stimulation, and very similar changes were observed in non-expressing neurons after electrical stimulation. This rules out that the changes in excitability observed were due to the opsin expression. An increase in cellular activity through cell-intrinsic mechanisms after prolonged firing agrees with many functional studies in vertebrates, using different experimental

excitability protocols (Abraham et al., 2019; Ryan et al., 2015; Titley et al., 2017). In fact, increases in excitability are also found following LTP induction in visual cortical neurons (Cudmore and Turrigiano, 2004), in hippocampal CA1 pyramidal cells (Xu, 2005), and after behavior training in CA1 (Disterhoft et al., 1986). Intrinsic excitability is also modified when an animal is exposed to novel sensorial experience (Brown et al., 2019) or after environmental enrichment (Valero-Aracama et al., 2015).

The intensity-dependent and persistent increase in firing rate after stimulation protocol could be due to changes in membrane resistance and firing threshold. The synergy between these mechanisms could make neurons reach firing threshold with smaller depolarizations. Thus, an increase in excitability would be particularly relevant for lower current injections generated by weaker inputs. We propose that, after optogenetic stimulation, neurons shift to a more excitable state, revealing weaker synaptic inputs and connections, like an iceberg emerging out of the water (Figure 8). Therefore, the same unchanged synaptic inputs could bring neurons to threshold and induce increased output firing after repetitive stimulation, improving their synaptic efficiency in postsynaptic pyramidal neurons (Debanne et al., 2019; Lisman et al., 2018; Nicoll et al., 1993; Titley et al., 2017; Zhang and Linden, 2003). Thus, neuronal optogenetic and electrical stimulation might alter the circuit without changing the synapses themselves, and this phenomenon could occur quickly.

Mechanisms of increased excitability in ensemble formation

Modifications in sub- and suprathreshold membrane conductances that initiate an action potential or a burst could underlie increased excitability (Brumberg et al., 2000). In terms of passive properties, our results coincide with many studies that have shown alterations in input resistance as the mechanism responsible for increases in excitability (Aizenman and Linden, 2000; Aou et al., 1992; Armano et al., 2000; Brown et al., 2019; Disterhoft et al., 1986; Marder and Goaillard, 2006; Woody et al., 1991; Xu, 2005). Activity-dependent increases in input resistance have been shown in hippocampal neurons. There, the increase in excitability could be potentiated by suppression of G protein-coupled inwardly rectifying K^+ channels (GIRK channels) (Valero-Aracama et al., 2015); or by cAMP-responsive element-binding protein (CREB)-dependent control of excitability by reducing K^+ conductance (Lisman et al., 2018; Yu et al., 2017). Additionally, the contribution of H-channels in intrinsic membrane properties (Campanac et al., 2008; Fan et al., 2005). However, that voltage sag, which corresponds to current-H, is largely absent in layer 2/3 pyramidal neurons (Kalmbach et al., 2018; van Aerde and Feldmeyer, 2015). Our experiment showed only a few neurons that displayed a modest current-H, but it was not affected by optogenetic or electrical stimulation (not shown).

Moreover, recent studies show that persisting firing could be mediated by an Ether-à-gogo Related Gene (ERG) K^+ channel in neocortical pyramidal neurons (Cui and Strowbridge, 2018; Debanne et al., 2019). In this view, calcium entry induced by repetitive activation could modulate leak potassium currents in the neurons, which will generate persistent activity. Consistent with this, in our experiments, the blockage of ERG channels by terfenadine returned the firing rate and the increased input resistance induced by optogenetic and electrical stimulation to basal conditions. Thus, ERG channels appear to have a tonic activity in pyramidal layer 2/3 neurons.

The cell-intrinsic mechanisms that induce excitability are cell-type and also, stimulation protocol-dependent (Angelo et al., 2012). Hence, different changes in action potential firing have been identified. One of the most common changes is a reduction in after-hyperpolarization (AHP) amplitude, described in hippocampal neurons (Disterhoft et al., 1986; Disterhoft and Oh, 2006; Malik and Chattarji, 2012; Pignatelli et al., 2019; Zhang and Linden, 2003). In our experiments, we found a significant decrease in spike threshold as the most robust change in optogenetic and electrical stimulated neurons. This parameter also determines the firing frequency of neurons associated with voltage-dependent sodium or calcium currents. Changes in threshold appear to be usual in cortical neurons after intrinsic plasticity induction (Brumberg et al., 2000; Cudmore and Turrigiano, 2004; Mahon and Charpier, 2012; Paz et al., 2009), hippocampal neurons (Malik and Chattarji, 2012; Valero-Aracama et al., 2015; Xu, 2005), and cerebellar Purkinje cells (Aizenman and Linden, 2000; Armano et al., 2000). Consistent with this, visual deprivation increases the spike threshold in the pyramidal neurons of the visual cortex, as an example of a mechanism that reduces neuronal excitability (Brown et al., 2019). It has been proposed that regulation of the persistent sodium current could underlie the lowering of spike threshold, throughout the modulation of protein kinase C (Astman et al., 1998; Valero-Aracama et al., 2015); or protein kinase A activation-dependent on calcium influx (Cudmore and Turrigiano, 2004). Also, potassium channels Kv1 can regulate the action potential threshold (Feria Pliego and Pedroarena, 2020). Therefore, the intrinsic plasticity by optogenetic stimulation that we report in pyramidal neurons from the visual cortex could result from modifications of voltage-gated ion channels and inward rectification by potassium channels. Future studies will examine the exact molecular mechanisms that underlying these increases in excitability.

Contribution of intrinsic excitability and synaptic plasticity to circuit plasticity

The apparently contradictory evidence supporting Hebbian synaptic plasticity or intrinsic mechanisms of circuit modification and ensemble formation could be reconciled if one considers the experimental protocol used, as well as temporal and mechanistic factors. As a note of caution, we should mention that the stimulation protocols we used are artificial, and the imprinting of ensembles with optogenetics or electrical stimulation may not be representative of the natural ensembles found and created in the cortex under physiological conditions. Thus, the balance of mechanisms we find may differ with *in vivo* ensembles, under naturalistic learning conditions. In particular, the optogenetic imprinting model for ensemble formation we used occurs quickly *in vivo*, as soon as we can measure it, within a few minutes. We also see fast changes in neuronal correlations *in vitro* after optogenetic and electrical stimulation. But this type of imprinted ensembles could be different from the circuit modification that occur during learning, which, for visual tasks, can take several days or weeks in the same circuit we study (Carrillo-Reid et al., 2019), and which could engage long-term plasticity, Hebbian or not Hebbian. In addition, intrinsic plasticity can underlie or contribute with Hebbian plasticity (Debanne et al., 2019). Thus, behavioral training could induce neuronal excitability through Hebbian mechanisms (Disterhoft et al., 1986; Malik and Chattarji, 2012; Valero-Aracama et al., 2015). So, circuit plasticity could be due to the interplay of synaptic and intrinsic mechanisms and this balance could be different for short and long-term plasticity. In this view that synthesizes all the different types of evidence, ensembles could be quickly formed by fast intrinsic mechanisms but then be modified by slower synaptic plasticity, perhaps in relation with learning.

To conclude, our work demonstrates that significant increases in cellular excitability by intrinsic mechanisms are found during ensemble formation induced by optogenetic and electrical stimulation. The possibility to modify input and output patterns in a postsynaptic neuron through changes in its firing properties could promote synaptic efficacy (Brumberg et al., 2000; Lisman, 1997) and increase the correlation between recruited neurons, as we have demonstrated. This could provide an ideal setting for Hebbian synaptic plasticity than could occur more slowly. Intrinsic excitability could also implement temporary stimulus-response mappings and might play a role in rapid cognitive flexibility (Pang and Fairhall, 2019). Faster “online” plasticity via intrinsic excitability could have a broad impact on network dynamics and could serve as a critical information-storage mechanism that may contribute to memory formation (Lisman et al., 2018; Marder and Goaillard, 2006; Pérez-Ortega et al., 2021; Pignatelli et al., 2019; Xu, 2005) and to the generation of intrinsic circuit states, such as for ensembles and circuit attractors (Buzsáki, 2010; Carrillo-Reid et al., 2019, 2016; Hopfield, 1982; Miller et al., 2014).

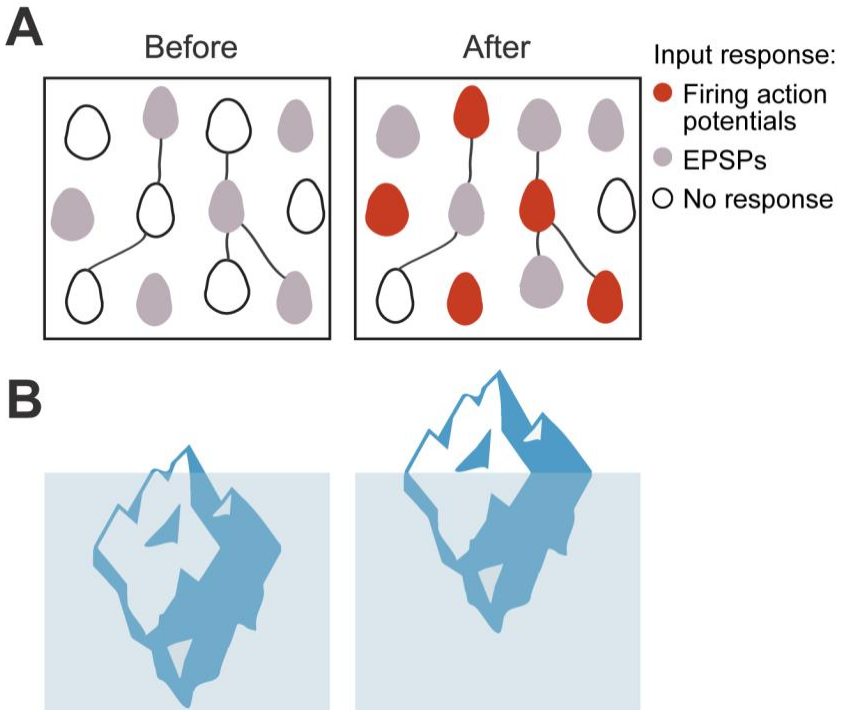

Figure 8. Iceberg model of ensemble formation.

(**A**) Emergence of ensembles after increases in neuronal excitability. Response of a neural circuit to a test input, before and after neurons are coactivated and increase their excitability. Color corresponds to membrane potential response to a synaptic input: white is resting membrane potentials, gray are subthreshold responses, and red are suprathreshold ones, with firing of action potentials. After stimulation, neurons become more excitable, so the same inputs induce some of them to fire (red cells), while other cells have increased subthreshold responses to the input (gray cells). The model can explain how an ensemble is formed but does not assume any changes in numbers of strength of synapses.

(**B**) Left: Iceberg emergence model: An iceberg keeps underwater. (Right) But if its weight decreases, the iceberg emerges above water. Weight (or density) is an intrinsic property of the iceberg and, by changing it, the iceberg changes its response to the same environment. Likewise, for a neuronal ensemble, membrane resistance and firing threshold are intrinsic neuronal

properties that can be modified, and they enhance its response to the same excitatory input intensity, resulting in an increased depolarization and generation of action potentials.

References

Abeles M. 1991. Corticonics. Cambridge University Press. doi:10.1017/CBO9780511574566

Abraham WC, Jones OD, Glanzman DL. 2019. Is plasticity of synapses the mechanism of long-term memory storage? *npj Science of Learning* **4**:9. doi:10.1038/s41539-019-0048-y

Aizenman CD, Linden DJ. 2000. Rapid, synaptically driven increases in the intrinsic excitability of cerebellar deep nuclear neurons. *Nature Neuroscience* **3**. doi:10.1038/72049

Angelo K, Rancz EA, Pimentel D, Hundahl C, Hannibal J, Fleischmann A, Pichler B, Margrie TW. 2012. A biophysical signature of network affiliation and sensory processing in mitral cells. *Nature* **488**:375–378. doi:10.1038/nature11291

Aou S, Woody C, Birt D. 1992. Increases in excitability of neurons of the motor cortex of cats after rapid acquisition of eye blink conditioning. *The Journal of Neuroscience* **12**. doi:10.1523/JNEUROSCI.12-02-00560.1992

Armano S, Rossi P, Taglietti V, D'Angelo E. 2000. Long-Term Potentiation of Intrinsic Excitability at the Mossy Fiber–Granule Cell Synapse of Rat Cerebellum. *The Journal of Neuroscience* **20**. doi:10.1523/JNEUROSCI.20-14-05208.2000

Astman N, Gutnick MJ, Fleidervish IA. 1998. Activation of Protein Kinase C Increases Neuronal Excitability by Regulating Persistent Na + Current in Mouse Neocortical Slices. *Journal of Neurophysiology* **80**:1547–1551. doi:10.1152/jn.1998.80.3.1547

Bliss TVP, Gardner-Medwin AR. 1973. Long-lasting potentiation of synaptic transmission in the dentate area of the unanaesthetized rabbit following stimulation of the perforant path. *The Journal of Physiology* **232**:357–374. doi:10.1113/jphysiol.1973.sp010274

Bliss TVP, Lømo T. 1973. Long-lasting potentiation of synaptic transmission in the dentate area of the anaesthetized rabbit following stimulation of the perforant path. *The Journal of Physiology* **232**. doi:10.1113/jphysiol.1973.sp010273

Brown APY, Cossell L, Margrie TW. 2019. Visual Experience Regulates the Intrinsic Excitability of Visual Cortical Neurons to Maintain Sensory Function. *Cell Reports* **27**:685-689.e4. doi:10.1016/j.celrep.2019.03.073

Brumberg JC, Nowak LG, McCormick DA. 2000. Ionic Mechanisms Underlying Repetitive High-Frequency Burst Firing in Supragranular Cortical Neurons. *Journal of Neuroscience* **20**:4829–4843. doi:10.1523/JNEUROSCI.20-13-04829.2000

Buzsáki G. 2010. Neural syntax: cell assemblies, synapsembles, and readers. *Neuron* **68**:362–85. doi:10.1016/j.neuron.2010.09.023

Campanac E, Daoudal G, Ankri N, Debanne D. 2008. Downregulation of Dendritic Ih in CA1 Pyramidal Neurons after LTP. *Journal of Neuroscience* **28**. doi:10.1523/JNEUROSCI.1411-08.2008

Carrillo-Reid L, Han S, Yang W, Akrouh A, Yuste R. 2019. Controlling Visually Guided Behavior by Holographic Recalling of Cortical Ensembles. *Cell* **178**:447-457.e5. doi:10.1016/j.cell.2019.05.045

Carrillo-Reid L, Yang W, Bando Y, Peterka DS, Yuste R. 2016. Imprinting and recalling cortical ensembles. *Science* **353**:691–694. doi:10.1126/science.aaf7560

Carter CA, Wojciechowski NJ, Hayes JM, Skoutakis VA, Rickman LA. 1985. Terfenadine, a Nonsedating Antihistamine. *Drug Intelligence & Clinical Pharmacy* **19**. doi:10.1177/106002808501901103

Churchland PS, Sejnowski TJ. 1992. The computational brain., The computational brain., Computational neuroscience. Cambridge, MA, US: The MIT Press.

Clopath C, Bonhoeffer T, Hübener M, Rose T. 2017. Variance and invariance of neuronal long-term representations. *Philosophical Transactions of the Royal Society B: Biological Sciences* **372**. doi:10.1098/rstb.2016.0161

Cossart R, Aronov D, Yuste R. 2003. Attractor dynamics of network UP states in the neocortex. *Nature* **423**:283–8. doi:10.1038/nature01614

Cossell L, Iacaruso MF, Muir DR, Houlton R, Sader EN, Ko H, Hofer SB, Mrsic-Flogel TD. 2015. Functional organization of excitatory synaptic strength in primary visual cortex. *Nature* **518**:399–403. doi:10.1038/nature14182

Cudmore RH, Turrigiano GG. 2004. Long-Term Potentiation of Intrinsic Excitability in LV Visual Cortical Neurons. *Journal of Neurophysiology* **92**:341–348. doi:10.1152/jn.01059.2003

Cui ED, Strowbridge BW. 2018. Modulation of Ether-à-Go-Go Related Gene (ERG) Current Governs Intrinsic Persistent Activity in Rodent Neocortical Pyramidal Cells. *Journal of Neuroscience* **38**:423–440. doi:10.1523/JNEUROSCI.1774-17.2017

dal Maschio M, Ghezzi D, Bony G, Alabastri A, Deidda G, Brondi M, Sato SS, Zaccaria RP, di Fabrizio E, Ratto GM, Cancedda L. 2012. High-performance and site-directed in utero electroporation by a triple-electrode probe. *Nature Communications* **3**:960. doi:10.1038/ncomms1961

Debanne D, Inglebert Y, Russier M. 2019. Plasticity of intrinsic neuronal excitability. *Current Opinion in Neurobiology* **54**:73–82. doi:10.1016/j.conb.2018.09.001

Desai NS, Rutherford LC, Turrigiano GG. 1999. Plasticity in the intrinsic excitability of cortical pyramidal neurons. *Nature Neuroscience* **2**. doi:10.1038/9165

Disterhoft JF, Coulter DA, Alkon DL. 1986. Conditioning-specific membrane changes of rabbit hippocampal neurons measured in vitro. *Proceedings of the National Academy of Sciences* **83**:2733–2737. doi:10.1073/PNAS.83.8.2733

Disterhoft JF, Oh MM. 2006. Learning, aging and intrinsic neuronal plasticity. *Trends in Neurosciences* **29**:587–599. doi:10.1016/j.tins.2006.08.005

Fan Y, Fricker D, Brager DH, Chen X, Lu H-C, Chitwood RA, Johnston D. 2005. Activity-dependent decrease of excitability in rat hippocampal neurons through increases in Ih. *Nature Neuroscience* **8**. doi:10.1038/nn1568

Feldmeyer D, Lübke J, Sakmann B. 2006. Efficacy and connectivity of intracolumnar pairs of layer 2/3 pyramidal cells in the barrel cortex of juvenile rats. *The Journal of Physiology* **575**. doi:10.1113/jphysiol.2006.105106

Feria Pliego JA, Pedroarena CM. 2020. Kv1 potassium channels control action potential firing of putative GABAergic deep cerebellar nuclear neurons. *Scientific Reports* **10**:6954. doi:10.1038/s41598-020-63583-7

Hamm JP, Peterka DS, Gogos JA, Yuste R. 2017. Altered Cortical Ensembles in Mouse Models of Schizophrenia. *Neuron* **94**:153-167.e8. doi:10.1016/j.neuron.2017.03.019

Hebb DO. 1949. The Organization of Behavior, New York: Wiley. doi:10.1016/S0361-9230(99)00182-3

Holmgren C, Harkany T, Svennenfors B, Zilberter Y. 2003. Pyramidal cell communication within local networks in layer 2/3 of rat neocortex. *The Journal of Physiology* **551**. doi:10.1113/jphysiol.2003.044784

Hopfield JJ. 1982. Neural networks and physical systems with emergent collective computational abilities. *Proceedings of the National Academy of Sciences of the United States of America* **79**:2554–8. doi:10.1073/pnas.79.8.2554

Hoshiba Y, Wada T, Hayashi-Takagi A. 2017. Synaptic Ensemble Underlying the Selection and Consolidation of Neuronal Circuits during Learning. *Frontiers in Neural Circuits* **11**. doi:10.3389/fncir.2017.00012

Hu H, Vervaeke K, Storm JF. 2002. Two forms of electrical resonance at theta frequencies, generated by M-current, h-current and persistent Na^+ current in rat hippocampal pyramidal cells. *The Journal of Physiology* **545**. doi:10.1113/jphysiol.2002.029249

Ikegaya Y. 2004. Synfire Chains and Cortical Songs: Temporal Modules of Cortical Activity. *Science* **304**:559–564. doi:10.1126/science.1093173

Johansson F, Jirenhed D-A, Rasmussen A, Zucca R, Hesslow G. 2014. Memory trace and timing mechanism localized to cerebellar Purkinje cells. *Proceedings of the National Academy of Sciences* **111**:14930–14934. doi:10.1073/pnas.1415371111

Juárez-Vidales J de J, Pérez-Ortega J, Lorea-Hernández JJ, Méndez-Salcido F, Peña-Ortega F. 2021. Configuration and dynamics of dominant inspiratory multineuronal activity patterns during eupnea and gasping generation in vitro. *Journal of Neurophysiology* **125**. doi:10.1152/jn.00563.2020

Kalmbach BE, Buchin A, Long B, Close J, Nandi A, Miller JA, Bakken TE, Hodge RD, Chong P, de Frates R, Dai K, Maltzer Z, Nicovich PR, Keene CD, Silbergeld DL, Gwinn RP, Cobbs C, Ko AL, Ojemann JG, Koch C, Anastassiou CA, Lein ES, Ting JT. 2018. h-Channels Contribute to Divergent Intrinsic Membrane Properties of Supragranular Pyramidal Neurons in Human versus Mouse Cerebral Cortex. *Neuron* **100**. doi:10.1016/j.neuron.2018.10.012

Kirkwood A, Rioult MG, Bear MF. 1996. Experience-dependent modification of synaptic plasticity in visual cortex. *Nature* **381**. doi:10.1038/381526a0

Ko H, Hofer SB, Pichler B, Buchanan KA, Sjöström PJ, Mrsic-Flogel TD. 2011. Functional specificity of local synaptic connections in neocortical networks. *Nature* **473**:87–91. doi:10.1038/nature09880

Lefort S, Tomm C, Floyd Sarria J-C, Petersen CCH. 2009. The Excitatory Neuronal Network of the C2 Barrel Column in Mouse Primary Somatosensory Cortex. *Neuron* **61**. doi:10.1016/j.neuron.2008.12.020

Levy RB, Reyes AD. 2012. Spatial Profile of Excitatory and Inhibitory Synaptic Connectivity in Mouse Primary Auditory Cortex. *Journal of Neuroscience* **32**. doi:10.1523/JNEUROSCI.5158-11.2012

Li B, Routh BN, Johnston D, Seidemann E, Priebe NJ. 2020. Voltage-Gated Intrinsic Conductances Shape the Input-Output Relationship of Cortical Neurons in Behaving Primate V1. *Neuron* **107**:185-196.e4. doi:10.1016/j.neuron.2020.04.001

Lisman J, Cooper K, Sehgal M, Silva AJ. 2018. Memory formation depends on both synapse-specific modifications of synaptic strength and cell-specific increases in excitability. *Nature Neuroscience* **21**:309–314. doi:10.1038/s41593-018-0076-6

Lisman JE. 1997. Bursts as a unit of neural information: making unreliable synapses reliable. *Trends in Neurosciences* **20**:38–43. doi:10.1016/S0166-2236(96)10070-9

Lorente De Nó R. 1938. Analysis of the activity of the chains of internuncial neurons. *Journal of Neurophysiology* **1**:207–244. doi:10.1152/jn.1938.1.3.207

Lorente de Nó R. 1933. Studies on the structure of the cerebral cortex. I. The area entorhinalis. *Journal für Psychologie und Neurologie*.

Mahon S, Charpier S. 2012. Bidirectional Plasticity of Intrinsic Excitability Controls Sensory Inputs Efficiency in Layer 5 Barrel Cortex Neurons in Vivo. *Journal of Neuroscience* **32**. doi:10.1523/JNEUROSCI.0415-12.2012

Malik R, Chattarji S. 2012. Enhanced intrinsic excitability and EPSP-spike coupling accompany enriched environment-induced facilitation of LTP in hippocampal CA1 pyramidal neurons. *Journal of Neurophysiology* **107**:1366–1378. doi:10.1152/jn.01009.2011

Manabe T, Renner P, Nicoll RA. 1992. Postsynaptic contribution to long-term potentiation revealed by the analysis of miniature synaptic currents. *Nature* **355**. doi:10.1038/355050a0

Marder E, Goaillard J-M. 2006. Variability, compensation and homeostasis in neuron and network function. *Nature Reviews Neuroscience* **7**:563–574. doi:10.1038/nrn1949

Mardinly AR, Oldenburg IA, Pégard NC, Sridharan S, Lyall EH, Chesnov K, Brohawn SG, Waller L, Adesnik H. 2018. Precise multimodal optical control of neural ensemble activity. *Nature Neuroscience* **21**:881–893. doi:10.1038/s41593-018-0139-8

Markram H, Lübke J, Frotscher M, Roth A, Sakmann B. 1997. Physiology and anatomy of synaptic connections between thick tufted pyramidal neurones in the developing rat neocortex. *The Journal of Physiology* **500**. doi:10.1113/jphysiol.1997.sp022031

Marshel JH, Kim YS, Machado TA, Quirin S, Benson B, Kadmon J, Raja C, Chibukhchyan A, Ramakrishnan C, Inoue M, Shane JC, McKnight DJ, Yoshizawa S, Kato HE, Ganguli S, Deisseroth K. 2019. Cortical layer-specific critical dynamics triggering perception. *Science (New York, NY)* **365**. doi:10.1126/science.aaw5202

Mellor J. 2002. Mediation of Hippocampal Mossy Fiber Long-Term Potentiation by Presynaptic Ih Channels. *Science* **295**. doi:10.1126/science.1064285

Miller J -e. K, Ayzenshtat I, Carrillo-Reid L, Yuste R. 2014. Visual stimuli recruit intrinsically generated cortical ensembles. *Proceedings of the National Academy of Sciences* **111**:E4053–E4061. doi:10.1073/pnas.1406077111

Morishima M, Morita K, Kubota Y, Kawaguchi Y. 2011. Highly Differentiated Projection-Specific Cortical Subnetworks. *Journal of Neuroscience* **31**. doi:10.1523/JNEUROSCI.0772-11.2011

Mrsic-Flogel TD, Hofer SB, Ohki K, Reid RC, Bonhoeffer T, Hübener M. 2007. Homeostatic Regulation of Eye-Specific Responses in Visual Cortex during Ocular Dominance Plasticity. *Neuron* **54**. doi:10.1016/j.neuron.2007.05.028

Narayanan R, Johnston D. 2008. The h Channel Mediates Location Dependence and Plasticity of Intrinsic Phase Response in Rat Hippocampal Neurons. *Journal of Neuroscience* **28**. doi:10.1523/JNEUROSCI.0835-08.2008

Nicoll A, Larkman A, Blakemore C. 1993. Modulation of EPSP shape and efficacy by intrinsic membrane conductances in rat neocortical pyramidal neurons in vitro. *The Journal of Physiology* **468**. doi:10.1113/jphysiol.1993.sp019795

Pang R, Fairhall AL. 2019. Fast and flexible sequence induction in spiking neural networks via rapid excitability changes. *eLife* **8**. doi:10.7554/eLife.44324

Paz JT, Mahon S, Tiret P, Genet S, Delord B, Charpier S. 2009. Multiple forms of activity-dependent intrinsic plasticity in layer V cortical neurones in vivo. *The Journal of Physiology* **587**:3189–3205. doi:10.1113/jphysiol.2009.169334

Penn AA, Shatz CJ. 1999. Brain Waves and Brain Wiring: The Role of Endogenous and Sensory-Driven Neural Activity in Development. *Pediatric Research* **45**:447–458. doi:10.1203/00006450-199904010-00001

Pérez-Ortega J, Alejandre-García T, Yuste R. 2021. Long-term stability of cortical ensembles. *eLife* **10**. doi:10.7554/eLife.64449

Pignatelli M, Ryan TJ, Roy DS, Lovett C, Smith LM, Muralidhar S, Tonegawa S. 2019. Engram Cell Excitability State Determines the Efficacy of Memory Retrieval. *Neuron* **101**:274-284.e5. doi:10.1016/j.neuron.2018.11.029

Ramón y Cajal S. 1909. Histologie du système nerveux de l'homme & des vertébrés. Paris : Maloine,. doi:10.5962/bhl.title.48637

Ross ST, Soltesz I. 2001. Long-term plasticity in interneurons of the dentate gyrus. *Proceedings of the National Academy of Sciences* **98**:8874. doi:10.1073/pnas.141042398

Ryan TJ, Roy DS, Pignatelli M, Arons A, Tonegawa S. 2015. Engram cells retain memory under retrograde amnesia. *Science* **348**:1007–1013. doi:10.1126/science.aaa5542

Sasaki T, Matsuki N, Ikegaya Y. 2007. Metastability of Active CA3 Networks. *Journal of Neuroscience* **27**:517–528. doi:10.1523/JNEUROSCI.4514-06.2007

Schneggenburger R, Sakaba T, Neher E. 2002. Vesicle pools and short-term synaptic depression: lessons from a large synapse. *Trends in Neurosciences* **25**:206–212. doi:10.1016/S0166-2236(02)02139-2

Schüz A, Braitenberg V. 2001. Cerebral Cortex: Organization and FunctionInternational Encyclopedia of the Social & Behavioral Sciences. Elsevier. pp. 1634–1640. doi:10.1016/B0-08-043076-7/03443-4

Sempere-Ferràndez A, Martínez S, Geijo-Barrientos E. 2019. Synaptic mechanisms underlying the intense firing of neocortical layer 5B pyramidal neurons in response to cortico-cortical inputs. *Brain Structure and Function* **224**. doi:10.1007/s00429-019-01842-8

Shepherd G. 2010. Handbook of Brain Microcircuits. Oxford University Press. doi:10.1093/med/9780195389883.001.0001

Shepherd GM. 2004. The Synaptic Organization of the Brain, The Synaptic Organization of the Brain. Oxford University Press. doi:10.1093/acprof:oso/9780195159561.001.1

Sjöström PJ, Rancz EA, Roth A, Häusser M. 2008. Dendritic Excitability and Synaptic Plasticity. *Physiological Reviews* **88**. doi:10.1152/physrev.00016.2007

Song S, Sjöström PJ, Reigl M, Nelson S, Chklovskii DB. 2005. Highly Nonrandom Features of Synaptic Connectivity in Local Cortical Circuits. *PLoS Biology* **3**. doi:10.1371/journal.pbio.0030068

Stringer C, Pachitariu M, Steinmetz N, Carandini M, Harris KD. 2019. High-dimensional geometry of population responses in visual cortex. *Nature* **571**:361–365. doi:10.1038/s41586-019-1346-5

Ting JT, Lee BR, Chong P, Soler-Llavina G, Cobbs C, Koch C, Zeng H, Lein E. 2018. Preparation of Acute Brain Slices Using an Optimized N-Methyl-D-glucamine Protective Recovery Method. *Journal of Visualized Experiments* e53825. doi:10.3791/53825

Titley HK, Brunel N, Hansel C. 2017. Toward a Neurocentric View of Learning. *Neuron* **95**:19–32. doi:10.1016/j.neuron.2017.05.021

Tonegawa S, Pignatelli M, Roy DS, Ryan TJ. 2015. Memory engram storage and retrieval. *Current Opinion in Neurobiology* **35**:101–109. doi:10.1016/j.conb.2015.07.009

Turrigiano G, Abbott L, Marder E. 1994. Activity-dependent changes in the intrinsic properties of cultured neurons. *Science* **264**. doi:10.1126/science.8178157

Turrigiano GG, Leslie KR, Desai NS, Rutherford LC, Nelson SB. 1998. Activity-dependent scaling of quantal amplitude in neocortical neurons. *Nature* **391**. doi:10.1038/36103

Valero-Aracama MJ, Sauvage MM, Yoshida M. 2015. Environmental enrichment modulates intrinsic cellular excitability of hippocampal CA1 pyramidal cells in a housing duration and anatomical location-dependent manner. *Behavioural Brain Research* **292**:209–218. doi:10.1016/J.BBR.2015.05.032

van Aerde KI, Feldmeyer D. 2015. Morphological and Physiological Characterization of Pyramidal Neuron Subtypes in Rat Medial Prefrontal Cortex. *Cerebral Cortex* **25**. doi:10.1093/cercor/bht278

Wandell BA, Smirnakis SM. 2009. Plasticity and stability of visual field maps in adult primary visual cortex. *Nature Reviews Neuroscience* **10**. doi:10.1038/nrn2741

Wiesel TN, Hubel DH. 1963. EFFECTS OF VISUAL DEPRIVATION ON MORPHOLOGY AND PHYSIOLOGY OF CELLS IN THE CAT'S LATERAL GENICULATE BODY. *Journal of Neurophysiology* **26**:978–993. doi:10.1152/jn.1963.26.6.978

Woody CD, Gruen E, Birt D. 1991. Changes in membrane currents during Pavlovian conditioning of single cortical neurons. *Brain Research* **539**. doi:10.1016/0006-8993(91)90688-R

Xu J. 2005. Activity-Dependent Long-Term Potentiation of Intrinsic Excitability in Hippocampal CA1 Pyramidal Neurons. *Journal of Neuroscience* **25**:1750–1760. doi:10.1523/JNEUROSCI.4217-04.2005

Yang Z, Santamaria F. 2016. Purkinje cell intrinsic excitability increases after synaptic long term depression. *Journal of Neurophysiology* **116**. doi:10.1152/jn.00369.2016

Yoshimura Y, Dantzker JLM, Callaway EM. 2005. Excitatory cortical neurons form fine-scale functional networks. *Nature* **433**. doi:10.1038/nature03252

Yu X-W, Oh MM, Disterhoft JF. 2017. CREB, cellular excitability, and cognition: Implications for aging. *Behavioural Brain Research* **322**:206–211. doi:10.1016/J.BBR.2016.07.042

Yuste R. 2015. From the neuron doctrine to neural networks. *Nature Reviews Neuroscience* **16**:487–497. doi:10.1038/nrn3962

Zhang LI, Poo M. 2001. Electrical activity and development of neural circuits. *Nature Neuroscience* **4**. doi:10.1038/nn753

Zhang W, Linden DJ. 2003. The other side of the engram: experience-driven changes in neuronal intrinsic excitability. *Nature Reviews Neuroscience* **4**. doi:10.1038/nrn1248